Solitary wave solutions and their interactions for fully nonlinear water waves with surface tension in the generalized Serre equations

Denys Dutykh, Mark Hoefer, Dimitrios Mitsotakis

Denys Dutykh
CNRS, Université Savoie Mont Blanc, France

Mark Hoefer
University of Colorado, USA

Dimitrios Mitsotakis
Victoria University of Wellington, New Zealand

Solitary wave solutions and their interactions for fully nonlinear water waves with surface tension in the generalized Serre equations

Last modified: February 11, 2017

Solitary wave solutions and their interactions for fully nonlinear water waves with surface tension in the generalized Serre equations

Denys Dutykh, Mark Hoefer, and Dimitrios Mitsotakis*

Abstract. Some effects of surface tension on fully-nonlinear, long, surface water waves are studied by numerical means. The differences between various solitary waves and their interactions in subcritical and supercritical surface tension regimes are presented. Analytical expressions for new peaked traveling wave solutions are presented in the case of critical surface tension. The numerical experiments were performed using a high-accurate finite element method based on smooth cubic splines and the four-stage, classical, explicit Runge–Kutta method of order four.

Key words and phrases: Serre equations; solitary waves; surface tension; peakons

MSC: [2010] 76B25 (primary), 76B15, 35Q51, 35C08 (secondary)
PACS: [2010] 47.35.Bb (primary), 47.35.Pq, 47.35.Fg (secondary)

Key words and phrases. Serre equations; solitary waves; surface tension; peakons.
* Corresponding author.

Contents

1. Introduction

In this paper, we numerically study the effects of surface tension on fully-nonlinear shallow-water waves. Surface water waves are usually described by the full EULER equations of water wave theory, [39]. Due to their complexity and the difficulties arising in their theoretical and numerical study, simpler model equations have been derived as approximations to the EULER equations in the shallow water regime. There are two often studied regimes within shallow water waves: (i) the weakly nonlinear – weakly dispersive and (ii) the fully nonlinear – weakly dispersive regime. Model equations such as weakly-nonlinear BOUSSINESQ systems modelling capillary–gravity waves in the regime (i) were derived in [13] (see also [14]). These models extend the BOUSSINESQ systems derived for surface waves with no surface tension in [4] and, although they incorporate surface tension effects, they are limited to small amplitude waves. Because of this approximation, some effects of surface tension cannot be observed due to the absence of higher-order nonlinear terms. For this reason, the study of higher-order models should be considered. Mathematical models appropriate for water waves with surface tension in the regime (ii) were derived in [17]. These equations extend the SERRE equations [34, 35], incorporating surface tension effects, and are referred to as the generalized SERRE (gSERRE) equations, *cf.* [17]. For the derivation, justification and generalisations of the model equations for surface water waves in both regimes we refer to [17, 24]. In this paper, we focus on the study of solitary wave solutions of the gSERRE equations.

We note that another higher order effect, dispersion, can play a fundamental role in the near critical surface tension regime, as in the fifth order KAWAHARA equation [22, 23] that describes weakly nonlinear, unidirectional shallow water waves. While higher order dispersion without surface tension for the fully nonlinear regime (ii) was recently presented in [29], its generalized, surface tension counterpart was only noted in [36] and has not been studied. Although additional model equations have been derived recently that incorporate more surface tension effects, [9, 10], we will restrict this study to the effects of surface tension on the solitary waves of the gSERRE equations.

The gSERRE system of equations is a very accurate mathematical model of shallow water waves derived as an approximation to the full EULER equations with surface tension and a flat bottom, [17, 24].

Here we consider a two-dimensional coordinate system $O\,x\,y$ with the horizontal axis coinciding with the still water level $y = 0$. A layer of a perfect, incompressible fluid (of constant density $\rho > 0$) is assumed to be bounded between a flat, impermeable bottom at $y = -d$ and its free surface $y = \eta(x,\,t)$ with air. In general, the gSerre equations can be obtained by also approximating the horizontal velocity $u\,(x,\,y,\,t)$ by the depth-averaged velocity and by approximating the pressure p jump across the interface using the small slope approximation $[\![p]\!] \approx -\sigma\,\eta_{x\,x}$. Following the general lines of [11], the gSERRE

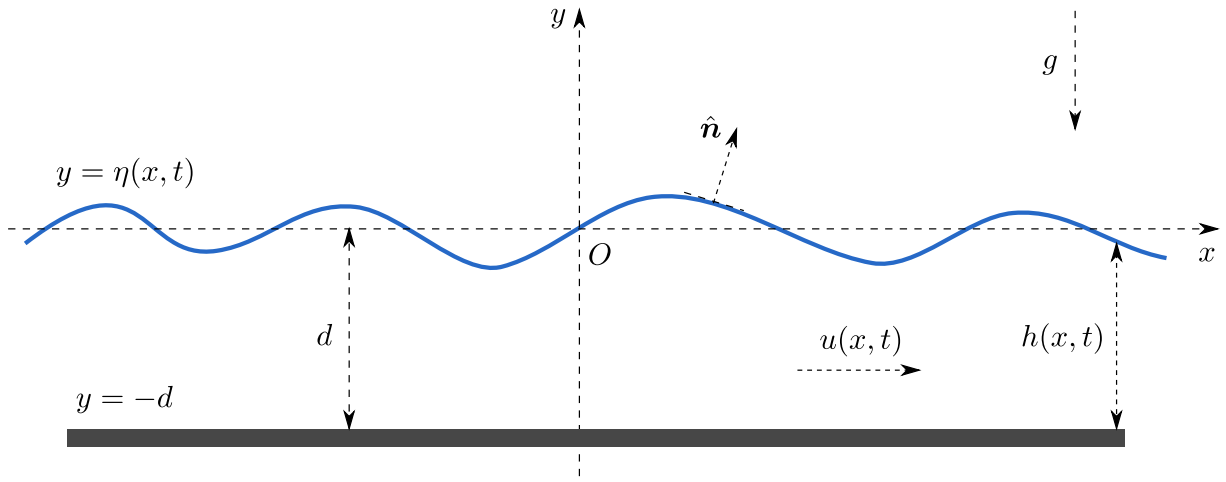

Figure 1. *Sketch of the fluid domain.*

equations then can be derived using variational methods (first derived in [17]) in the form:

$$h_t + [hu]_x = 0 \,, \tag{1.1}$$

$$u_t + u\,u_x + g h_x = \frac{1}{3h}\left[h^3\left(u_{xt} + u\,u_{xx} - u_x^2\right)\right]_x + \tau\, h_{xxx} \,. \tag{1.2}$$

or in non-dimensional but unscaled form (for brevity, we use the same variable names for nondimensional quantities):

$$h_t + [hu]_x = 0 \,, \tag{1.3}$$

$$h\,u_t + h\,h_x + h\,u\,u_x - \frac{1}{3}\left[h^3\left(u_{xt} + uu_{xx} - (u_x)^2\right]_x - B\,h\,h_{xxx} = 0 \,, \tag{1.4}$$

where both variables $h\,(x,\,t)$ and $u\,(x,\,t)$ are functions of the spatial x and temporal t variables. The function $h\,(x,\,t) = 1 + \eta\,(x,\,t)$ denotes the total depth from the bottom $d = -1$ up to the water's free surface η. The depth-averaged horizontal water velocity is denoted by u. The Bond number measures the ratio of gravity to capillary forces and can be defined as $\tau = \sigma/\rho$, where σ is the surface tension coefficient, ρ the constant density of the fluid, [21]. We will utilize the dimensionless Bond number in the form $B = \tau/gd^2 \geqslant 0$. When $B = 0$ (*i.e.* no surface tension is considered) then the gSerre equations (1.3), (1.4) reduce to the Serre equations.

An important, structural property of the gSerre equations is their linear dispersion relation $\omega^2 = k^2(1 + Bk^2)/(1 + k^2/3)$. For $B = 0$, the dispersion curvature $\omega''(k)$ is single-signed for positive wavenumbers k. The dispersion is convex (or concave). For $B > 0$, the dispersion relation is non-convex, exhibiting an inflection point at $k_* = \sqrt{3}\sqrt{1 + \sqrt{(1+B)/B}}$. This loss of dispersion convexity can have important physical implications, for example on solitary waves, [9, 22] and undular bores [36]. This feature makes the gSerre equations particularly interesting for further study. When $B = 1/3$, the dispersion relation is degenerate $\omega^2 = k^2$ and the gSerre equations are no longer dispersive, designating $B = 1/3$ as a critical value of surface tension.

Several conservation laws can also be derived for the gSERRE system in a similar way as in the case of the SERRE equations. Here we only mention four of these conservation laws:

$$\left[u - \frac{(h^3 u_x)_x}{3h}\right]_t + \left[\frac{u^2}{2} + gh - \frac{h^2 u_x^2}{2} - \frac{u(h^3 u_x)_x}{3h} - \tau h_{xx}\right]_x = 0\,, \tag{1.5}$$

$$\left[hu - \frac{(h^3 u_x)_x}{3}\right]_t + \left[hu^2 + \frac{gh^2}{2} - \frac{2h^3 u_x^2}{3} - \frac{h^3 u u_{xx}}{3} - h^2 h_x u u_x - \tau \mathcal{R}\right]_x = 0\,, \tag{1.6}$$

$$[hu]_t + \left[hu^2 + \tfrac{1}{2}gh^2 + \tfrac{1}{3}h^2\gamma - \tau\mathcal{R}\right]_x = 0, \tag{1.7}$$

$$\left[\frac{hu^2}{2} + \frac{h^3 u_x^2}{6} + \frac{gh^2}{2} + \frac{\tau}{2}h_x^2\right]_t + \left[\left(\frac{u^2}{2} + \frac{h^2 u_x^2}{6} + gh + \frac{h\gamma}{3} - \tau h_{xx}\right)hu + \tau h_x (hu)_x\right]_x = 0, \tag{1.8}$$

where we introduced two quantities: $\gamma = h\left[u_x^2 - u_{xt} - u\,u_{xx}\right]$, $\mathcal{R} = h\,h_{xx} - \frac{1}{2}h_x^2$. The quantity γ can be considered physically as the vertical acceleration of fluid particles computed at the free surface.

It is known that the SERRE equations admit solitary wave solutions of elevation type (*i.e.* of sech^2-type), [2]. Capillary effects have been shown to be important for the shape of the solitary waves, [17, 19]. Specifically, the presence of surface tension makes an elevation solitary wave narrower than a solitary wave of the SERRE equations with the same speed. Moreover, depending on the value of the BOND number B, the solitary waves can be either of elevation or of depression type. Depression solitary waves have negative excursion relative to the fluid background. The critical BOND number where the nature of the solitary wave changes, has been found to be $B = 1/3$, [17]. For $B < 1/3$ the gSERRE equations admit elevation solitary waves while for $B > 1/3$ they admit depression solitary waves. It is noted that there are no known analytical formulas for solitary waves of the gSERRE equations and for this reason numerical computations are required. The change in the physical properties of the fluid that depends on the value of the BOND number near the critical value $B = 1/3$ has been observed in the full water wave equations too, *cf. e.g.* [5, 15, 16]. As it was also suggested in [5, 36] we may expect some interesting phenomena around the critical BOND number $B = 1/3$.

The SERRE equations (without capillary effects) were first derived in [34, 35] and rederived various times since then, *cf., e.g.* [37]. Although there exist several studies, both theoretical and numerical, for the SERRE equations without surface tension, [20, 31] the behaviour of solitary waves under the effects of surface tension remain unknown, [17]. This paper is focused on the properties of solitary wave solutions of the gSERRE equations with surface tension and, in general, how surface tension influences their dynamics. Special attention has been given to the critical value of the BOND number $B = 1/3$, where it is shown that the gSERRE equations admit peaked solitary waves of elevation (peakons) and

depression (antipeakons) type. The equations (1.3) – (1.4) are solved numerically in a periodic domain using the standard GALERKIN/Finite element method of [33]. The numerical method used has been proven very efficient with optimal convergence rates [1, 33].

The paper is organized as follows. In Section 2, we present the numerical methods used in this paper along with their numerical validation. Section 3 contains numerical results which analyse the various interactions between elevation and depression solitary waves for multiple values of the BOND number B. Finally, the main conclusions are discussed in Section 4.

2. Numerical methods

Consider the gSERRE equations (1.3) – (1.4) in their dimensionless but unscaled form with $g = 1$. Lacking analytical expressions for gSERRE solitary waves, we present an efficient numerical method for their numerical generation. Then, the standard GALERKIN/finite element method is presented for the numerical integration of the gSERRE equations.

2.1. Numerical computation of solitary waves

It is known that the SERRE equations possess solitary wave solutions traveling at constant speed c_s of the form $h(x,t) = 1 + \eta_s(x - c_s t)$, $u(x,t) = u_s(x - c_s t)$ with $\eta_s(\xi) = A\,\mathrm{sech}^2[\lambda\xi]$, $u_s(\xi) = 1 - 1/(1 + \eta_s(\xi))$, $\lambda = \sqrt{3A/(4(1+A))}$ and $c_s = \sqrt{1+A}$.

On the other hand, it was shown in [17] that the gSERRE equations possess classical solitary wave solutions that satisfy the ordinary differential equation

$$\eta' = \pm\eta\sqrt{\frac{c_s^2 - 1 - \eta}{c_s^2/3 - B(\eta+1)}}\,, \tag{2.1}$$

while they share the same relation between u and η, *i.e.* $u = 1 - 1/(1+\eta)$ with the SERRE equations. They also share the same speed-amplitude relation $A = c_s^2 - 1$.

Without loss of generality, we search for solitary waves that are positive and symmetric about $x = 0$ for $0 \leqslant B < 1/3$. We consider a large enough interval $x \in [-L, L]$ so that the solitary wave has decayed sufficiently close to the background value $\eta = 1$ within this interval. A nonuniform grid of $[0, L]$ is used, $0 = x_0 < x_1 < \cdots < x_N = L$, where we assume that the function η is decreasing on this grid. Integration of (2.1) yields

$$-\int_{\eta(0)}^{\eta(x_i)} \frac{1}{\eta}\sqrt{\frac{c_s^2/3 - B(\eta+1)}{c_s^2 - 1 - \eta}}\,\mathrm{d}\eta = \int_0^{x_i}\mathrm{d}x\,. \tag{2.2}$$

Making the change of variable $\eta = \exp(z)$, then (2.2) can be simplified to the equation

$$\int_{\log\eta(x_i)}^{\log\eta(0)}\sqrt{\frac{c_s^2/3 - B(\exp(z)+1)}{c_s^2 - 1 - \exp(z)}}\,\mathrm{d}z - x_i = 0\,, \tag{2.3}$$

which defines the values $\eta_i = \eta(x_i)$ implicitly. Gauss–Legendre numerical quadrature is used for the approximation of the integral in (2.3) while the resulting nonlinear equations are solved with the secant method for values η_i in the interval $(0, c_s^2 - 1]$. Usually, the secant method converges in several iterations for a relative error tolerance of $\mathcal{O}(10^{-10})$. For the nodes x_i, we used the quadrature nodes of the Gauss–Legendre quadrature rule in a uniform grid of the computational domain. It is noted that the discretization of the inner products in the Finite Element method is based on Gauss–Legendre quadrature and therefore the numerically generated solitary waves can be used directly without using interpolation.

From Equation (2.1), we observe that the case where $B = 1/3$ is a singular case and no solitary waves can be generated numerically using the present method. On the other hand, the linear dispersion relation of the gSerre equations are degenerate for $B = 1/3$, with no linear dispersion. This implies that the asymptotic approximation of full water waves has broken down and higher order dispersion should be taken into account, [22]. On the other hand, one can verify that the solution

$$\eta(x,t) = A\,\exp(-\kappa\,|\xi|) \quad \text{with} \quad \kappa = \sqrt{3} \tag{2.4}$$

satisfies (2.1) with $B = 1/3$. Therefore, the critical gSerre equations with $B = 1/3$ possess peakons of elevation and depression type since the formula is valid for any $A \neq 0$, [6, 32].

2.2. Numerical time integration of the gSerre equations

For the numerical approximation of the initial value problem of the gSerre equations subject to periodic boundary conditions, we implement a standard Galerkin / finite element method for the spatial discretization and the fourth-order, four-stage classical Runge–Kutta method for the discretization in time (*cf.* [33] for the Serre equations lacking surface tension). Consider the system (1.3) – (1.4) posed in a finite interval $[a, b]$ and for time $t \in [0, T]$ with some $T > 0$, and with periodic boundary conditions, *i.e.* $h^{(k)}(a, t) = h^{(k)}(b, t)$ and $u^{(k)}(a, t) = u^{(k)}(b, t)$ for $k = 0, 1, 2, \ldots$. We consider a uniform subdivision of the interval $[a, b]$ consisting of the nodes $x_i = a + i\,\Delta x$, where $i = 0, 1, \cdots, N$, and $N \in \mathbb{N}$, such that the grid size is defined as $\Delta x = (b - a)/N$. We shall consider numerical solutions of the gSerre equations in the space of cubic, periodic splines

$$S = \{\phi \in C^2_{per}[a, b] \,\big|\, \phi|_{[x_i, x_{i+1}]} \in \mathbb{P}^3, \quad 0 \leqslant i \leqslant N - 1\},$$

where

$$C^2_{per} = \{f \in C^2[a, b] \,\big|\, f^{(k)}(a) = f^{(k)}(b), \quad 0 \leqslant k \leqslant 2\},$$

and $\mathbb{P}^3$ is the space of cubic polynomials.

The numerical solution will be denoted by $\tilde{h}$ and $\tilde{u}$. To state the spatial Galerkin semi-discretization, we first multiply equations (1.3) – (1.4) with $\phi \in S$. Integration by

parts leads to the weak formulation:

$$(\tilde{h}_t,\, \phi) \;+\; ((\tilde{h}\,\tilde{u})_x,\, \phi) \;=\; 0\,, \tag{2.5}$$

$$\mathcal{B}\,(\tilde{u}_t,\, \phi;\, \tilde{h}) \;+\; (\tilde{h}\,(\tilde{h}_x \;+\; \tilde{u}\,\tilde{u}_x),\, \phi) \;+\; \frac{1}{3}\,\Big(\tilde{h}^3\,(\tilde{u}\,\tilde{u}_{xx} \;-\; (\tilde{u}_x)^2),\, \phi_x\Big)$$
$$+\; B\,\Big[(\tilde{h}\,\tilde{h}_{xx},\, \phi_x) \;+\; (\tilde{h}_x\,\tilde{h}_{xx},\, \phi)\Big] \;=\; 0\,, \tag{2.6}$$

where the bilinear form $\mathcal{B}$ is defined for a fixed $\tilde{h}$ (and $\phi,\, \psi \;\in\; S$) as

$$\mathcal{B}(\psi,\, \phi;\, \tilde{h}) \;=\; (\tilde{h}\,\psi,\, \phi) \;+\; \frac{1}{3}\,(\tilde{h}^3\,\psi_x,\, \phi_x)\,, \tag{2.7}$$

and the initial conditions are

$$\tilde{h}\,(x,\, 0) \;=\; P\,h_0\,(x)\,, \qquad \tilde{u}\,(x,\, 0) \;=\; P\,u_0\,(x)\,, \tag{2.8}$$

where P is the L^2 projection onto S defined by $(Pv,\, \phi) \;=\; (v,\, \phi)$, for all $\phi \;\in\; S$.

Using the standard basis functions with B-splines for the space S, the equations (2.5) – (2.6) form a system of ordinary differential equations. It has been shown that the classical, explicit, four-stage, fourth-order Runge–Kutta method performs very well for the surface tensionless Serre equations, [33]. Denoting by Δt the uniform time-step, we consider the temporal grid $t^n \;=\; n\,\Delta t$, for $n \;=\; 0,\, 1,\, \cdots,\, K$, with $\Delta t \;=\; T/K$. For more information about the formulation and properties of this fully-discrete scheme, we refer the reader to [1, 33]. For the numerical computation of the integrals appearing in the numerical method, we use the Gauss–Legendre quadrature rule with five nodes. The nodes of the quadrature rule form a nonuniform grid which we used in the numerical method presented in Section 2.1.

2.3. Method validation

In order to validate the presented numerical methods for solitary wave computation and time integration, we generated and numerically evolved solitary wave solutions for various values of the Bond number B. As it was noted in [17], solitary waves for $B \;<\; 1/3$ are of elevation type while for $B \;>\; 1/3$ are of depression type, *cf.* Figure 2. Solitary waves are computed on the domain $[\,-40,\, 40\,]$. Figure 2 presents a magnification of the numerically generated solitary waves for various values of the Bond number B along with an exact solitary wave of the Serre system with $c_s \;=\; 1.5$.

In order to study the accuracy of the approximation of the solitary waves, we used the numerically generated solitary waves for $B \;=\; 0.1$ and $B \;=\; 0.5$ as initial conditions to the fully discrete numerical time integration scheme and studied several error indicators relevant to the propagation of traveling waves. Specifically, we monitored the amplitude, speed, shape and phase errors for solitary wave propagation up to time $T \;=\; 100$. It is noted that for elevation solitary waves we used the discretization parameters $\Delta x \;=\; 0.1$ and $\Delta t \;=\; 0.05$, while for depression solitary waves we used smaller mesh lengths $\Delta x \;=\; 0.01$ and $\Delta t \;=\; 0.005$ in order to produce stable and accurate computations.

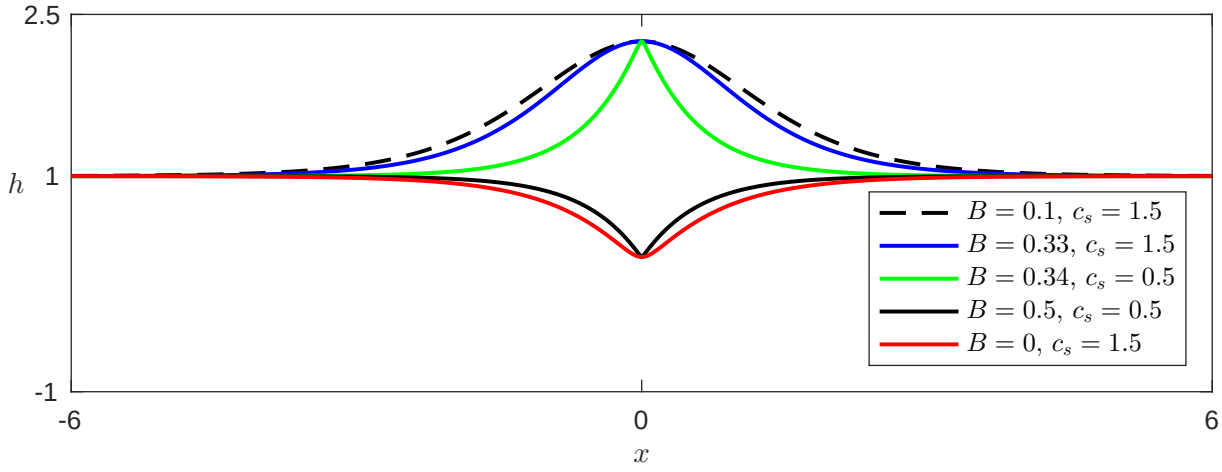

Figure 2. *Numerically computed solitary waves for the* gSERRE *equations with various values of* BOND *number* B .

We define the normalized amplitude error as

$$E_{amp} \;=\; \frac{|\, H(x^*(t),\, t) \;-\; H_0\,|}{|\, H_0\,|}\;, \tag{2.9}$$

where $x^*\,(t)$ is the curve along which the computed approximate solution $H\,(x,\,t)$ achieves its maximum and $H_0 \;\equiv\; H\,(0)$ is the initial peak amplitude of the numerically generated solitary wave. We observe that E_{amp} remains very small and practically constant during the propagation of the solitary waves, *cf.* Figure 3.

Additionally, we approximate the solitary wave speed c_s by $\tilde{c}_s$ as

$$\tilde{c}_s \;=\; \frac{x^*(t) \;-\; x^*\,(t-\tau)}{\tau}\;, \tag{2.10}$$

where τ is a constant. The corresponding speed error is defined as

$$E_{speed} \;=\; \frac{\tilde{c}_s \;-\; c_s}{c_s}\;.$$

The results for $\tau \;=\; 10$ in Figure 3 show that the error between the numerical values $\tilde{c}_s$ and the exact speed c_s remained practically constant.

Two other error norms that are pertinent to solitary waves are the *shape and phase errors*. We define the normalized shape error as the distance in L^2 between the computed solution at time $t \;=\; t^n$ and the family of translated, exact solitary waves with the same amplitude/speed, *i.e.*,

$$E_{shape} \;=\; \min_{\tau}\zeta(\tau)\;,\quad \zeta\,(\tau) \;=\; \frac{\|\, H(x,\,t^n) \;-\; h(x,\,\tau)\,\|}{\|\, h\,(x,0)\,\|}\;. \tag{2.11}$$

The minimum in (2.11) is attained at some critical $\tau \;=\; \tau^*\,(t^n)$. This, in turn, is used to define the (signed) phase error as

$$E_{phase} \;=\; \tau^* \;-\; t^n\,. \tag{2.12}$$

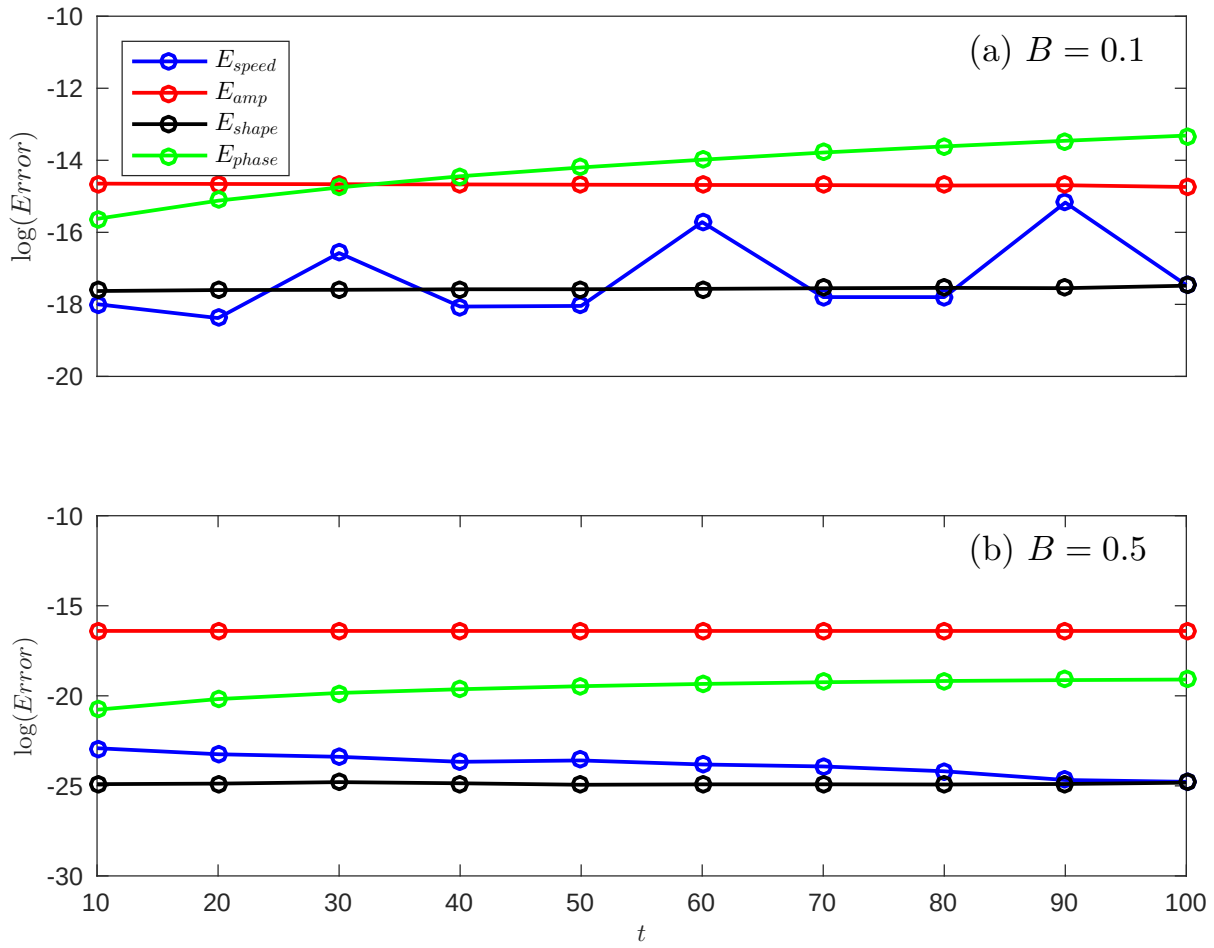

Figure 3. *Error indicators for the propagation of two solitary waves.*

In order to find τ^*, we solve the equation $\zeta'(\tau) = 0$ using NEWTON's method. The initial guess for NEWTON's method is chosen as $\tau^0 = t^n - \Delta t$. Having computed τ^*, the shape error (2.11) is then

$$E_{shape} = \zeta(\tau^*) .$$

These error norms are closely related to the *orbit* of the solitary wave and measure properties of the solitary waves, which are often not well conserved using dissipative numerical methods.

The computed numerical errors are presented on a logarithmic scale in Figure 3. It can be observed that the errors in the propagation of both solitary waves are very small. Especially when we use grids with small Δx, the numerical speed of propagation of the solitary wave was almost equal to the exact speed and similarly the rest of the error indicators remained very small. This study shows that both numerical methods are very accurate and they conserve the properties of a propagating solitary wave very well. We note that the errors are analogous for solitary waves with different propagation speeds since they primarily depend on the discretization Δx and Δt. We also mention that the

fully-discrete scheme appeared to be stable with no restrictive bounds on the ratio $\Delta t/\Delta x$ except when the solution is not very smooth. Mild restrictions, empirically found to be on the order $\Delta t/\Delta x \lessapprox 10^{-2}$, could be necessary for the numerical stability of the solution.

As the Bond number B approaches the value $1/3$, solitary wave solutions become more cusp-shaped, approaching the peakon solution (2.4), *cf.* Figure 2. For example, the solitary waves for $B = 0.33$ are very close to peaked solitary waves, [6, 27]. As the solitary waves lose smoothness, then the mesh length Δx must be reduced in order to maintain high resolution. We discuss further the transcritical case where $B \approx 1/3$ in Section 3.

3. Numerical experiments

In this section, we study the effects of surface tension on various solitary wave interactions. Specifically, we study the head-on and overtaking collisions of elevation and depression solitary waves. We also study the generation and interaction of solitary waves when the Bond number $B \approx 1/3$.

3.1. Head-on collisions

We first study the symmetric head-on collision for the gSerre equations with $B = 0.1$ for two identical elevation solitary waves that propagate in opposite directions. In these numerical experiments with elevation solitary waves, we consider the interval $[-200, 200]$ and take $\Delta x = 0.1$, $\Delta t = 0.01$. Here we present the solitary waves with $c_s = 1.2$ and amplitude $A = 0.4472$. The solitary waves are initially translated so that their maximum values are achieved at $x = -50$ and $x = 50$, respectively, exhibiting essentially no overlap in their exponentially small tails. The interaction begins at approximately $t = 40$ and the peak of the interaction occurs at about $t = 42$. The interaction is presented in Figure 4. We observe that after the collision, the solitary waves propagate in different directions followed by small amplitude dispersive tails.

In addition to the generation of dispersive tails, the inelastic interaction causes a phase change in the propagation of the solitary waves. During the collision there is a temporal interval in which the solution has only one peak while the maximum value of the solution during the interaction recorded was 0.9838, which is greater than the sum of the amplitudes, 0.88, of the solitary waves. The solitary waves after the interaction are separated and stabilized to different amplitudes $A \approx 0.4377$ compared with the initial amplitudes $A = 0.4472$.

Figure 5 shows the amplitude (a) and the location of the maximum values of the solution (b) recorded during the interaction. We observe that, due to nonlinear interaction, the amplitude fluctuates before it is stabilized to its new value. The dotted lines in these diagrams represent the solitary wave maximum if there was no interaction.

We performed several symmetric head-on collisions and recorded the maximum value at $x = 0$ during the interaction. This value is also known as the maximum runup since,

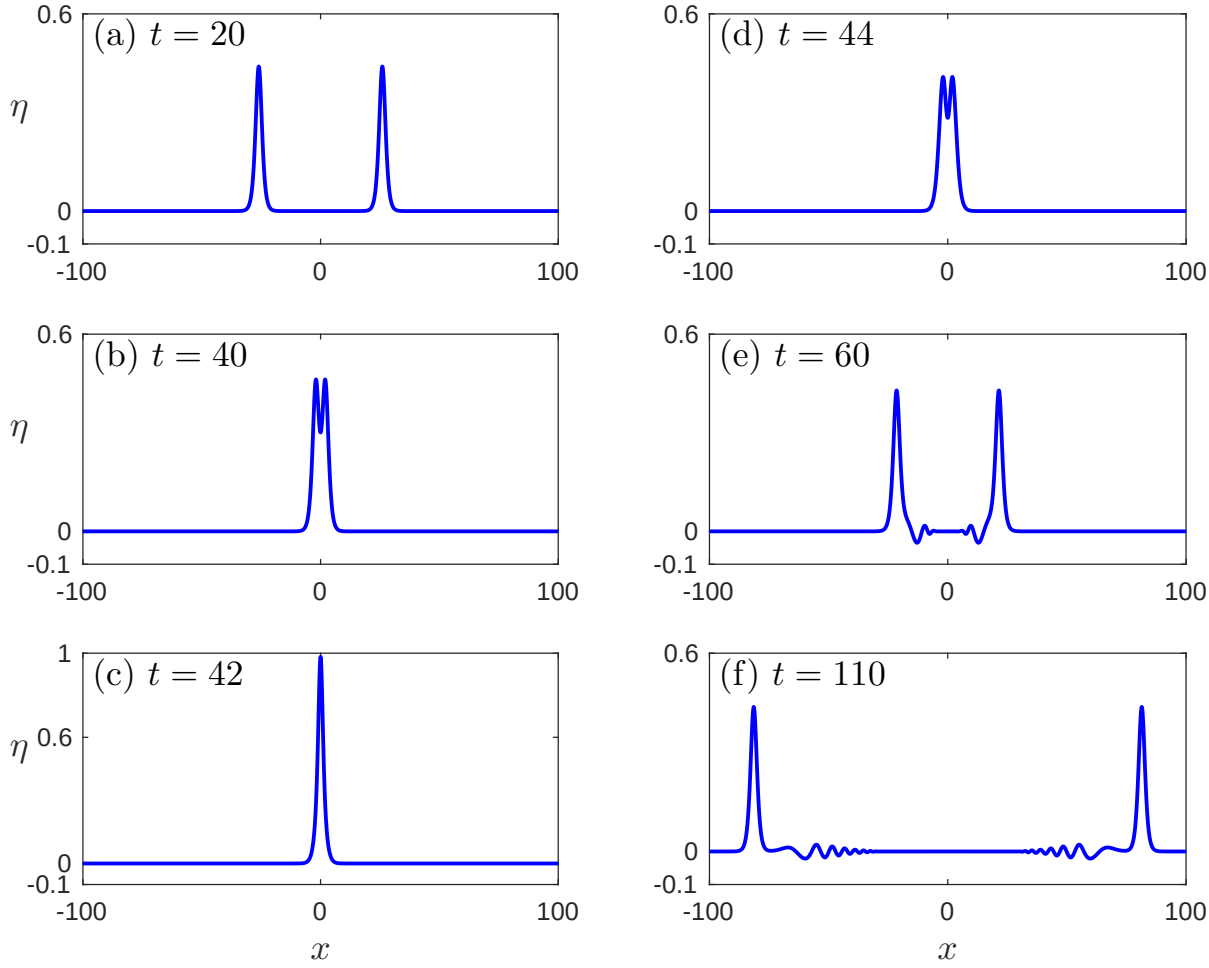

Figure 4. *Symmetric head-on collision of two elevation solitary waves for the* g*Serre equations with* $B = 0.1$.

by reflection symmetry $h(x, t) = h(-x, t)$, $u(x, t) = -u(x, t)$ of the equations and the initial data, it coincides with the maximum runup of a solitary wave on a vertical wall located at $x = 0$ subject to appropriate boundary conditions [31, 38]. Figure 6 shows the values recorded for $B = 0.2$ and 0.3 compared with the asymptotic solution of [31] for $B = 0$. We observe that surface tension decreases the maximum runup value. This effect is stronger for larger amplitude solitary waves for the same values of B. Moreover, the maximum runup value is decreasing with B. Therefore, for larger values of B, we observe smaller maximum runup values.

We also studied the unsymmetric collision of two solitary waves with amplitudes $A = 0.96$ and 0.44, respectively (equivalently, speeds 1.4 and 1.2, respectively). The interaction is very similar to the unsymmetric interaction of the Serre equations and is not presented here. We only mention that the solitary waves after the interaction have amplitudes $A \approx 0.9515$ and 0.4325 respectively. In conclusion, the head-on collision of elevation solitary

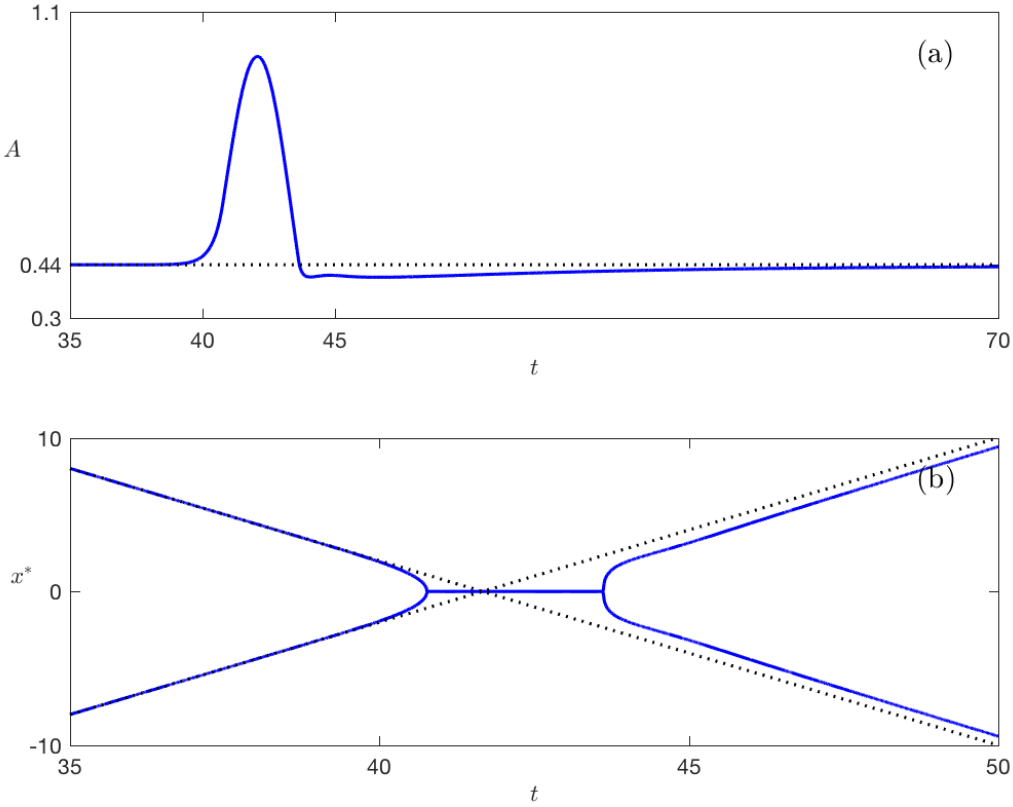

Figure 5. *(a) Peak amplitude of the solution as a function of time, (b) Phase diagram of the location of the solitary waves during the interaction of Figure 4.*

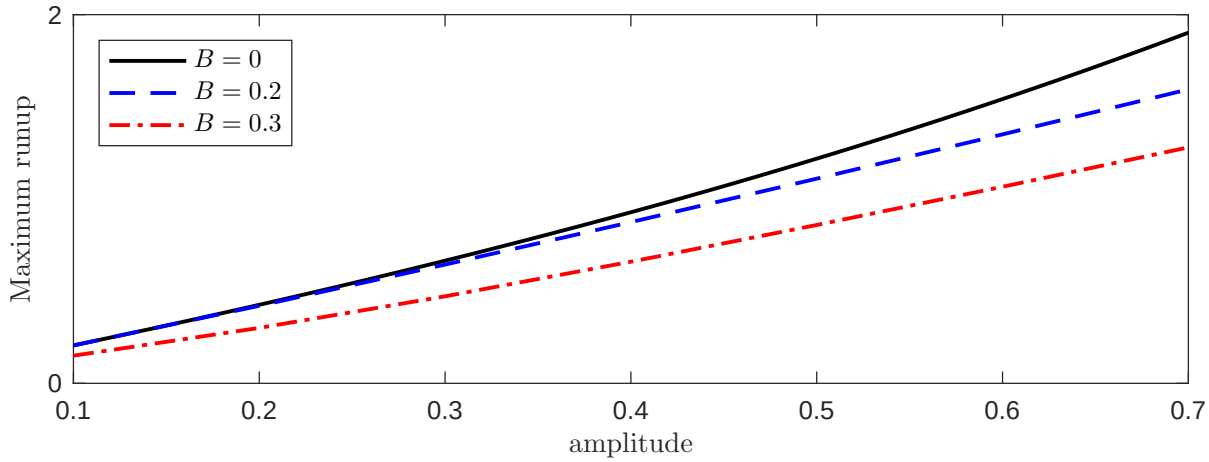

Figure 6. *Maximum runup of solitary waves for* $B = 0, 0.2$ *and* 0.3.

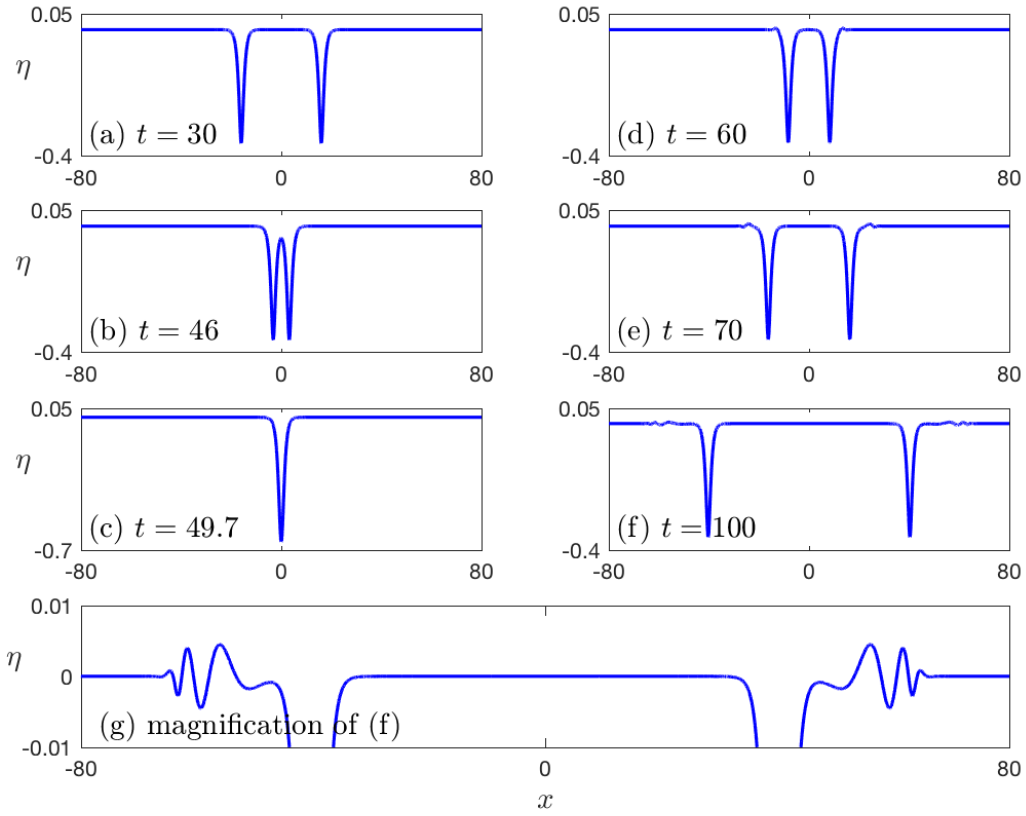

Figure 7. *Symmetric head-on collision of two depression solitary waves for the* g*Serre equations with* $B = 0.5$.

waves with small surface tension is qualitatively the same as the collision of solitary waves with no surface tension. It is noted that a jet formation can be observed during the head-on collision of large amplitude solitary waves. [7, 8]. This jet formation is very difficult to be observed by the gSerre equations since the solution must be a function.

We continue with the head-on collision of depression solitary waves for Bond number greater than $1/3$. The interaction of depression solitary waves has never been studied before and there are no previous results to compare with. We studied the symmetric head-on collision of two solitary waves of speed $c_s = 0.8$ and amplitude $A = -0.36$ (where we keep the minus sign to emphasise that the solution is negative) for Bond number $B = 0.5$. Initially, the solitary waves were translated to $x = -40$ and 40 respectively and we solved the gSerre equations in the interval $[-100, 100]$ with $\Delta x = 0.01$ and $\Delta t = 0.001$. Figure 7 shows the inelastic interaction between two depression solitary waves. It is interesting that the dispersive tails generated after the interaction propagate faster than the solitary waves and therefore lead in the propagation while there are no deviations of the free surface between the two new solitary pulses.

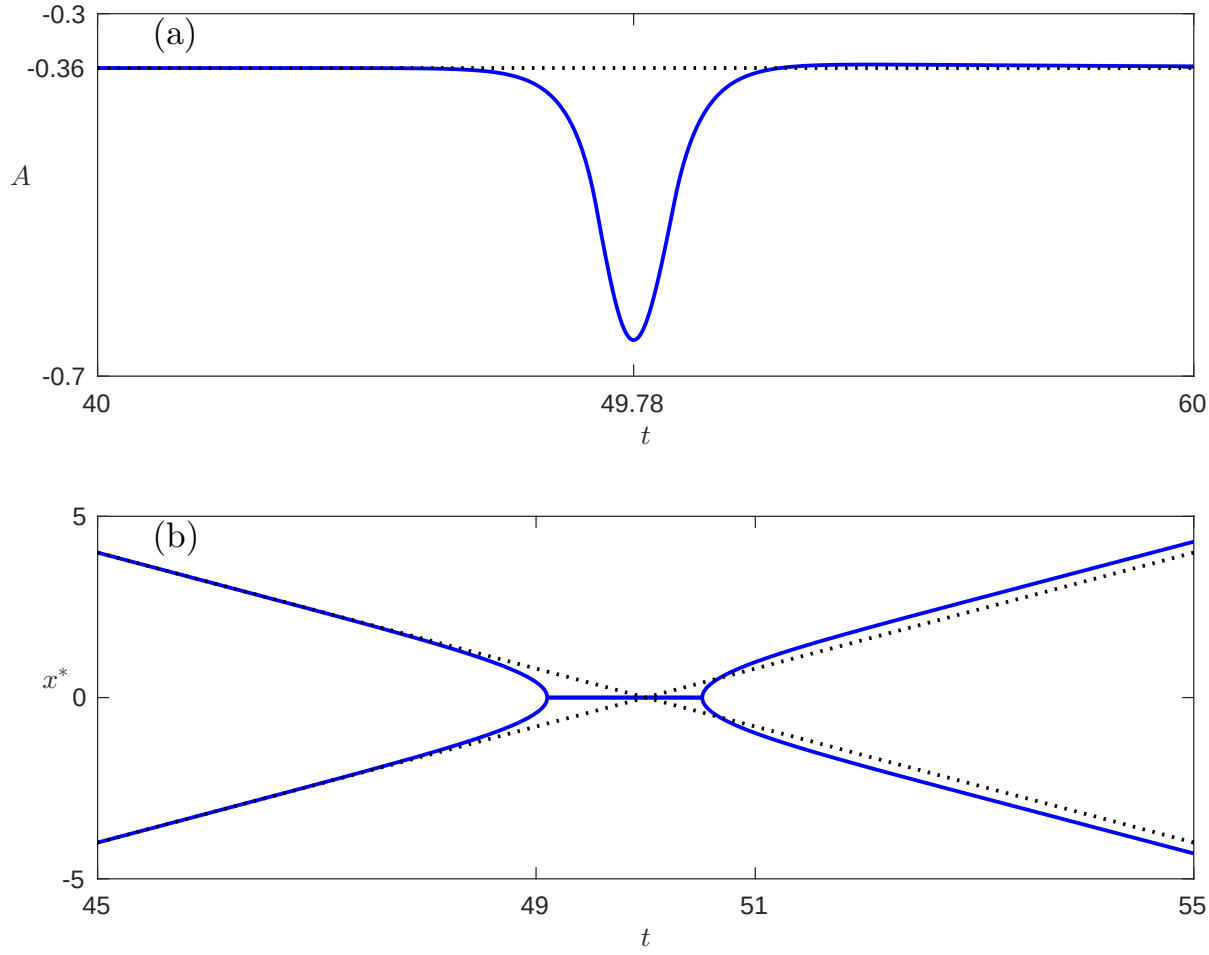

Figure 8. *(a) Peak amplitude of the solution as a function of time, (b) Phase diagram of the location of the solitary waves during the interaction of Figure 7.*

The minimum peak amplitude of the solution -0.66 was recorded at about $t = 49.78$. This value is larger than the sum of the peak amplitudes of the two solitary waves. Because of the nonlinear interaction, a phase shift can be observed in both pulses, but here the resulting solitary waves have larger amplitude $A \approx -0.3598$ and therefore propagate faster than the initial solitary waves. Also, the phase change is different than the subcritical case $B < 1/3$. In the supercritical case $B > 1/3$, the waves travel faster during the interaction and were separated earlier compared to the case where small or no surface tension is considered. The minimum of the solution as a function of time and the phase diagram with the location of the peak amplitudes of the solitary waves are presented in Figure 8. The effect of strong surface tension $B > 1/3$ on the head-on collision of solitary waves is to invert the dynamics of the collision relative to the weak surface tension case $B < 1/3$, resulting in faster solitary waves and dispersive tails propagating faster than the solitary waves.

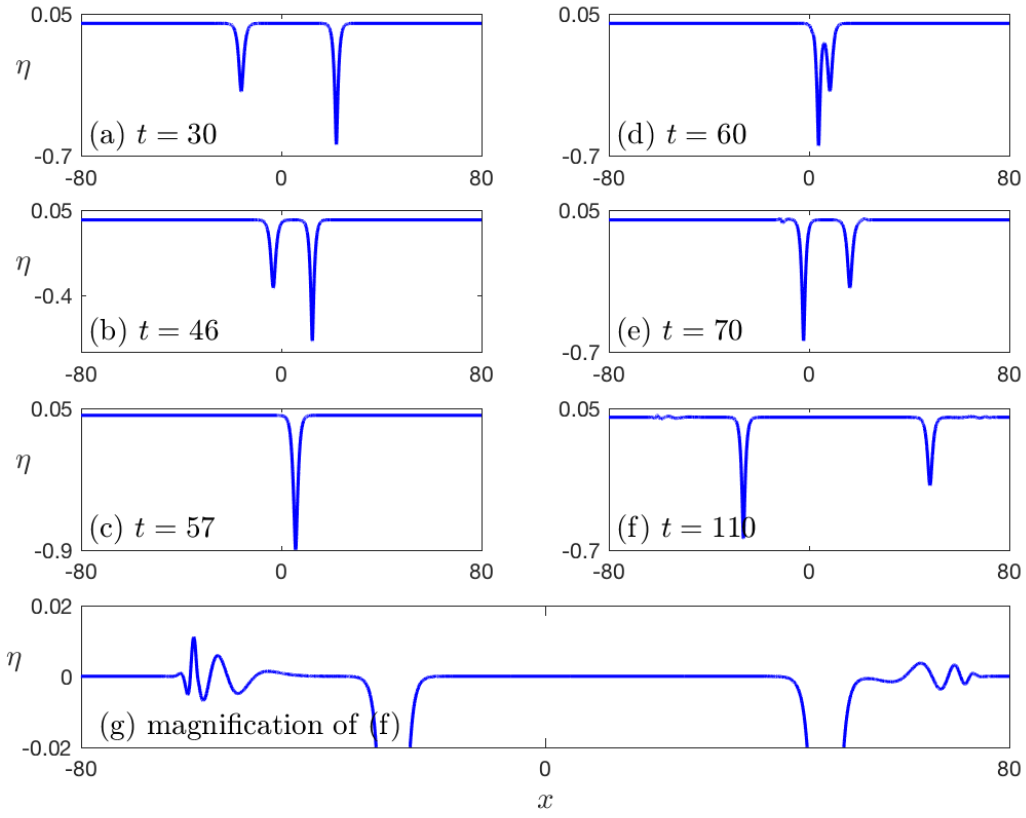

Figure 9. *Unsymmetric head-on collision of two solitary waves for the g*SERRE *equations with* $B = 0.5$.

The collision of two solitary waves of unequal size is very similar to the one with solitary waves of equal amplitudes. For example, we consider solitary waves with speeds $c_s = 0.6$ and 0.8 corresponding to amplitudes $A = -0.36$ and -0.64, respectively. The results of the inelastic collision are presented in Figure 9. The dispersive tails are traveling faster than the solitary pulses again but now their shape is different, having deformed to solitary waves with different amplitudes post interaction: $A \approx -0.35974$ and $A \approx -0.63958$. The evolution of the minimum value of the solution is very similar with the one presented in Figure 8 and so it is omitted.

3.2. Overtaking collisions

We now consider a different type of interaction, the overtaking collision of two solitary waves traveling in the same direction but with different speeds. In contrast to the head-on collision case, the overtaking interaction is often referred to as the *strong interaction* of

solitary waves due to the relative importance of nonlinearity [30]. For the Korteweg–de Vries (KdV) equation, a standard weakly nonlinear, long wave model of unidirectional waves, there are three categories of overtaking collisions classified by Lax [25]. Each category corresponds to a distinct geometry of solitary wave interaction. These categories have been observed in experiment and computation of fully nonlinear water wave models (Euler and Serre equations) [1, 12] and in experiment and a model of viscous core-annular flows [28]. Here, we will consider the Lax categories within the context of the gSerre equations for various Bond numbers.

We label the three categories (a), (b), and (c). Lax category (a) corresponds to solitary waves of similar size whose interaction remains bimodal throughout, resulting in a small exchange of mass from the larger to the smaller solitary wave. In Lax category (c), the small solitary wave is absorbed completely by the large solitary wave, resulting in a symmetric, unimodal conglomerate at the peak of interaction. Following this, the smaller solitary wave is ejected behind the larger wave and each propagates independently. Lax category (b) is a combination of categories (a) and (c). In this case, the two solitary waves initially form an asymmetric, unimodal mass. At the peak of interaction, however, the conglomerate is bimodal. This process is undone and the smaller solitary wave is emitted behind the larger wave.

In what follows, we denote the amplitudes A_1, A_2 for the larger and smaller solitary waves, respectively. The amplitude ratio is denoted $r = A_1/A_2 > 1$. For the KdV equation, interactions with $r \leqslant (3+\sqrt{5})/2$ are category (a), with $(3+\sqrt{5})/2 < r < 3$ are category (b) and with $r \geqslant 3$ are category (c).

It is important to not that the Lax categories for the KdV equation are completely determined by the amplitude ration r of the two solitons. This is because the KdV equation admits Galilean scaling invariances that enable one to fix the leading, slower soliton to have amplitude 1 and trailing, faster soliton to amplitude r, both on a zero background. While the gSerre equations admit Galilean and scaling symmetries, the Lax categories for two soliton interactions functionally depend on both soliton amplitudes A_1 and A_2 separately. This is because the scaling symmetry is used to fix the total water height, here normalised to unity. In what follows, we fix the amplitude of the faster gSerre soliton to unity $A_1 = 1$ and vary the slower soliton's amplitude $A_2 < 1$ in order to identify the Lax categories in this restricted regime. Therefore, we consider the ration $r = 1/A_2$, [12, 28].

In the first case with Bond number $B = 0.2$ similar types of interactions were observed. We used 3 decimal digits in the calculation of the parameter r and we observed that interactions with $r \leqslant 3.453$ are in the category (a), for $3.469 \leqslant r \leqslant 5.129$ they are in the category (b) and for $r \geqslant 5.130$ they are in the category (c). For values of r in the interval $[\,3.453,\, 3.468\,]$ we observed a transition zone between categories (a) and (b) where the small solitary wave was absorbed and re-emitted only after the exchange of the masses towards the end of the interaction. This phenomenon has been observed also in the case of the overtaking collisions of the Serre equations with $3.097 \leqslant r \leqslant 3.108$, [1]. The limits for the three Lax categories for the Serre equations as reported in [1], along with the limits for the gSerre (with $B = 0.2$) and Euler equations, [12], are summarised in

Lax categories	(a)	(b)	(c)
Euler	$r \leqslant 2.941$	$2.941 < r \leqslant 3.536$	$r > 3.536$
Serre	$r \leqslant 3.096$	$3.109 \leqslant r \leqslant 3.978$	$r \geqslant 3.979$
gSerre	$r \leqslant 3.453$	$3.469 \leqslant r \leqslant 5.129$	$r \geqslant 5.130$

Table 1. Lax *categories for the* Euler, Serre *and* gSerre *equations with* $B = 0.2$.

Table 1 (for $A_1 = 1$). It is noted that the values presented in Table 1 are correct to the digits shown and are approximate values, so they can used as an indication of where the transition is happening.

Phase diagrams of the different interactions of the solitary waves in each of the Lax categories are presented in Figure 10. In Figure 10 (a) we observe that the two solitary waves keep a distance while they exchange masses. It is also easy to observe the absorption of the small solitary wave in Figure 10(b) and (c). The dotted lines represent the paths of the solitary waves as if there were no interaction.

The interaction with $r = 2.5$ in the Lax category (a) is depicted in Figure 11 where it is shown that during the interaction there are two peaks. In Figure 12 the interaction with $r = 4$ in the Lax category (b) is presented where the small solitary wave is absorbed by the large solitary wave initially and then is re-emitted and two peaks are present during the interaction, while in the end is absorbed again and finally ejected and separated from the large solitary wave. Figure 13 shows the interaction with $r = 10$, which belongs to the Lax category (c) and where during the interaction only one peak can be observed as the small solitary wave is absorbed by the large one until it is ejected and separated from the large one at the end of the interaction.

The maximum value of the solution as a function of time for several values of r is presented in Figure 14. We observe that the maximum of the solution during the interaction does not behave monotonically with r. So we can achieve the same maximum for different values of r. For large values of r and in the category (c) of Lax, the amplitude as a function of time is a smooth function. In the categories (a) and (b) the maximum appeared to have a singularity at the time t where the minimum is occurred.

Although the limits for the Lax categories of overtaking collisions are different when surface tension is included (*cf.*, Table 1) the interactions are very similar and no new phenomena were observed when compared to the results reported in [1, 12, 26, 31, 33].

Like in the case of the Serre equations, small amplitude dispersive tails were generated during and after the interaction of two solitary waves. The dispersive tails are propagating mainly to the right but a small $N-$shaped wavelet is generated and propagates to the left as shown in Figure 15.

We draw the conclusion that the overtaking collision of two solitary waves for the gSerre equations with $B < 1/3$ retains the qualitative characteristics of the analogous interaction for the Serre equations. The situation for the gSerre equations with $B > 1/3$ is very

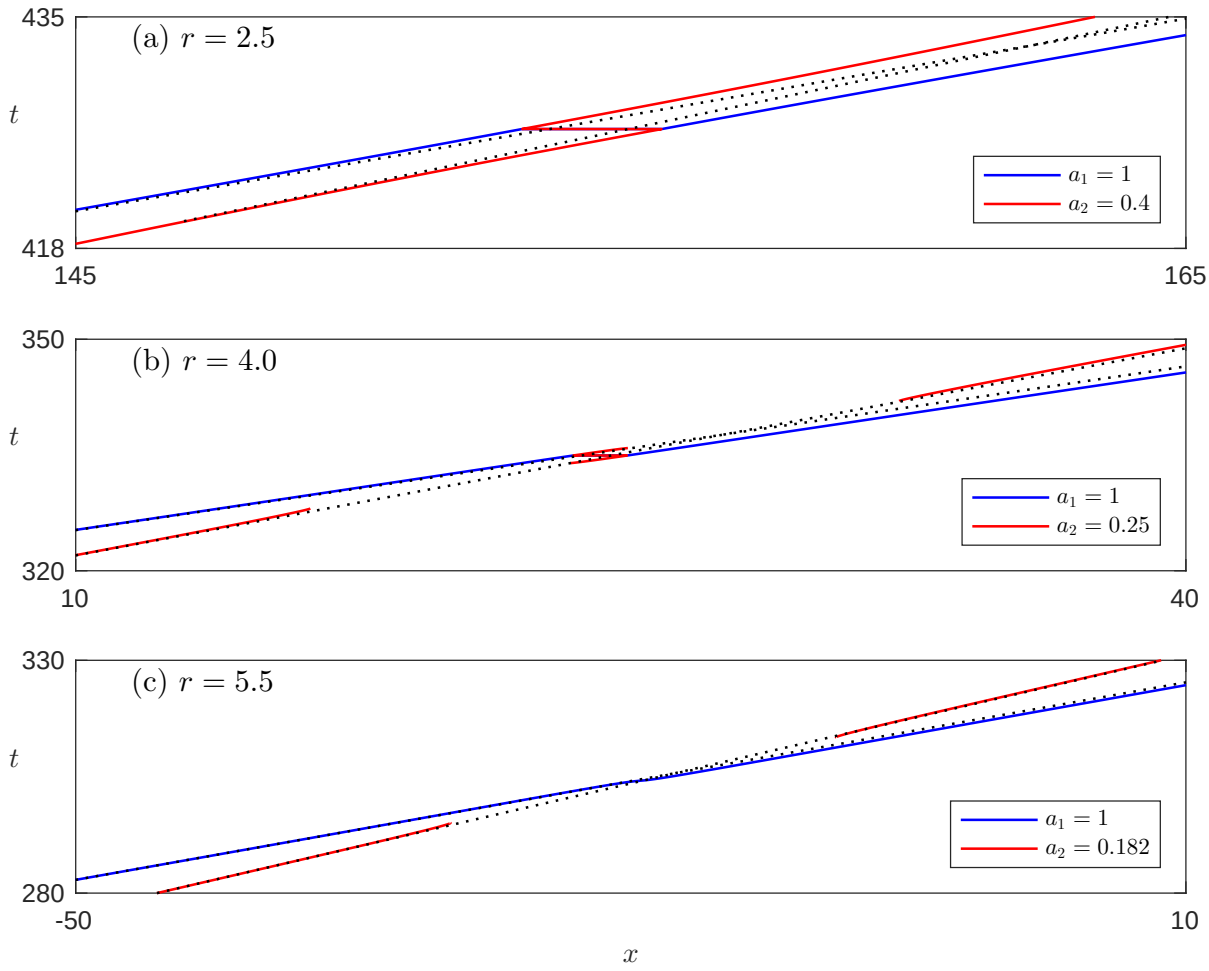

Figure 10. *Phase diagrams of the three categories of* Lax *for the overtaking collision of two elevation solitary waves of the g*Serre *equations with* $B = 0.2$.

different and interesting where new phenomena can be observed, as we now demonstrate. Again we consider the gSerre equations with $B = 0.5$ and we test overtaking collisions for different solitary waves. In this case, again we were able to observe the analogous three categories of Lax but here, the values of r are totally different and cannot be compared with the analogous results obtained for small values of Bond number B. Specifically, we define here $r = a_2/a_1$ with $a_1 > a_2$ *i.e.* the amplitude of the small solitary wave over the amplitude of the large solitary wave.

In order to compare numerical results with the predictions of Lax, we restrict our attention to solitary waves of small amplitude where the unidirectional solitary waves of the gSerre equations can be asymptotically approximated by KdV solitary waves. All the experiments were performed in $[-200, 200]$ and the solitary waves were translated initially so as to attain their maximum values at $x = -50$ and $x = 50$ respectively.

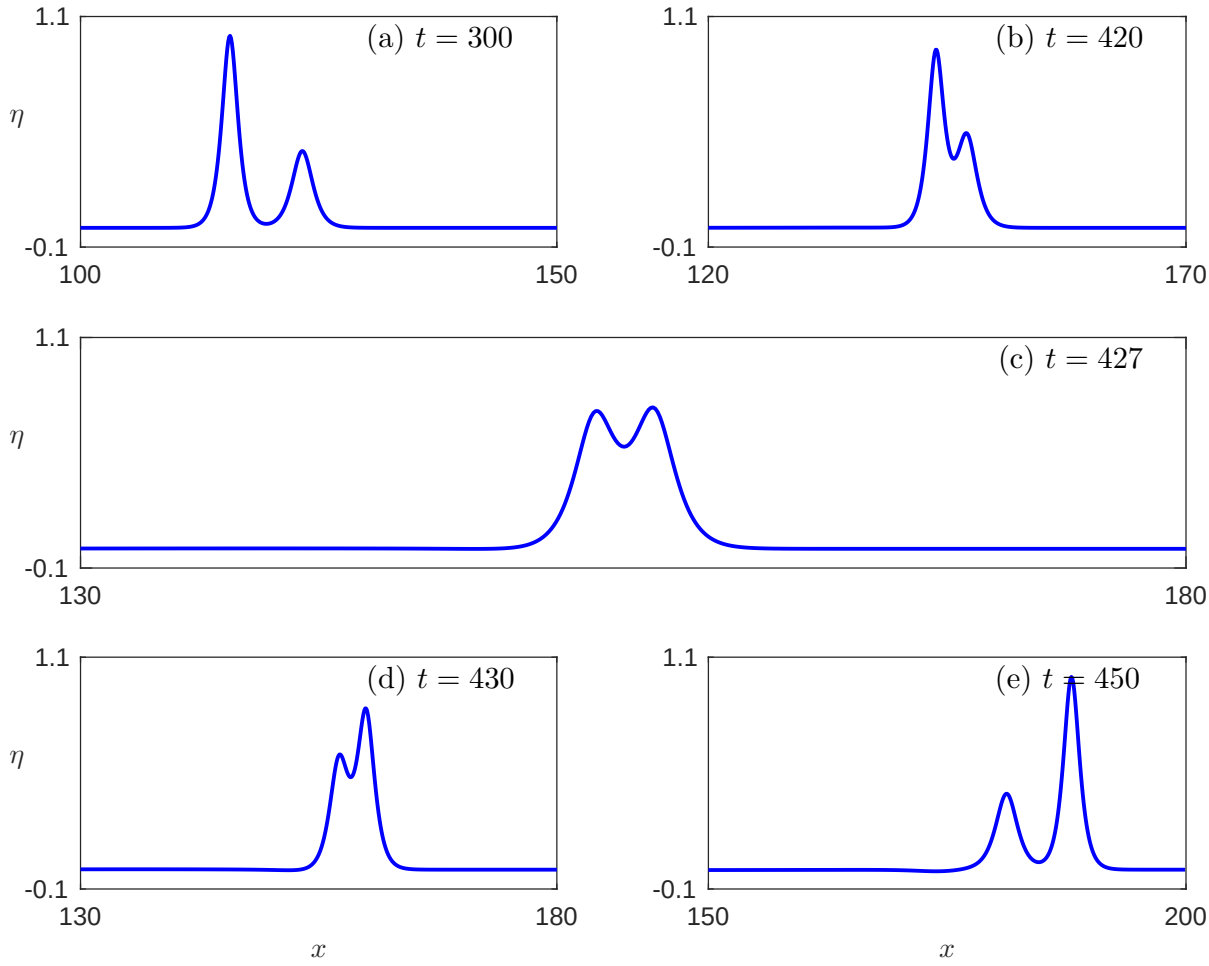

Figure 11. *Interaction of two solitary waves with* $r = 2.5$ *of the* g SERRE *equations with* $B = 0.2$. LAX *category (a).*

When $B < 1/3$ we took $\Delta x = 0.1$ and $\Delta t = 0.01$ while, when $B > 1/3$ we took $\Delta x = 0.02$ and $\Delta t = 0.01$.

In these experiments the fast solitary wave has amplitude $a_1 = -0.1$. Then for a small solitary wave of amplitude $a_2 = -0.2$ the interaction falls into the LAX category (a). As it can be observed in Figure 16, the solitary waves exchange masses and there are always two pulses present in the domain. On the other hand, when we took $a_2 = -0.3$, the small solitary wave was initially absorbed by the large solitary wave, and then re-emitted, causing the existence of two local minima during the interaction, as described by LAX category (b). Finally, for $a_2 = -0.4$ the small solitary wave is absorbed by the large one during the interaction and after the interaction is ejected and separated from the large one.

Again, the minimum value of the solution as a function of time behaves similarly to the case of small BOND number but here the amplitude is the negative minimum of the solution. Figure 19 shows the evolution of the amplitude as a function of time for different

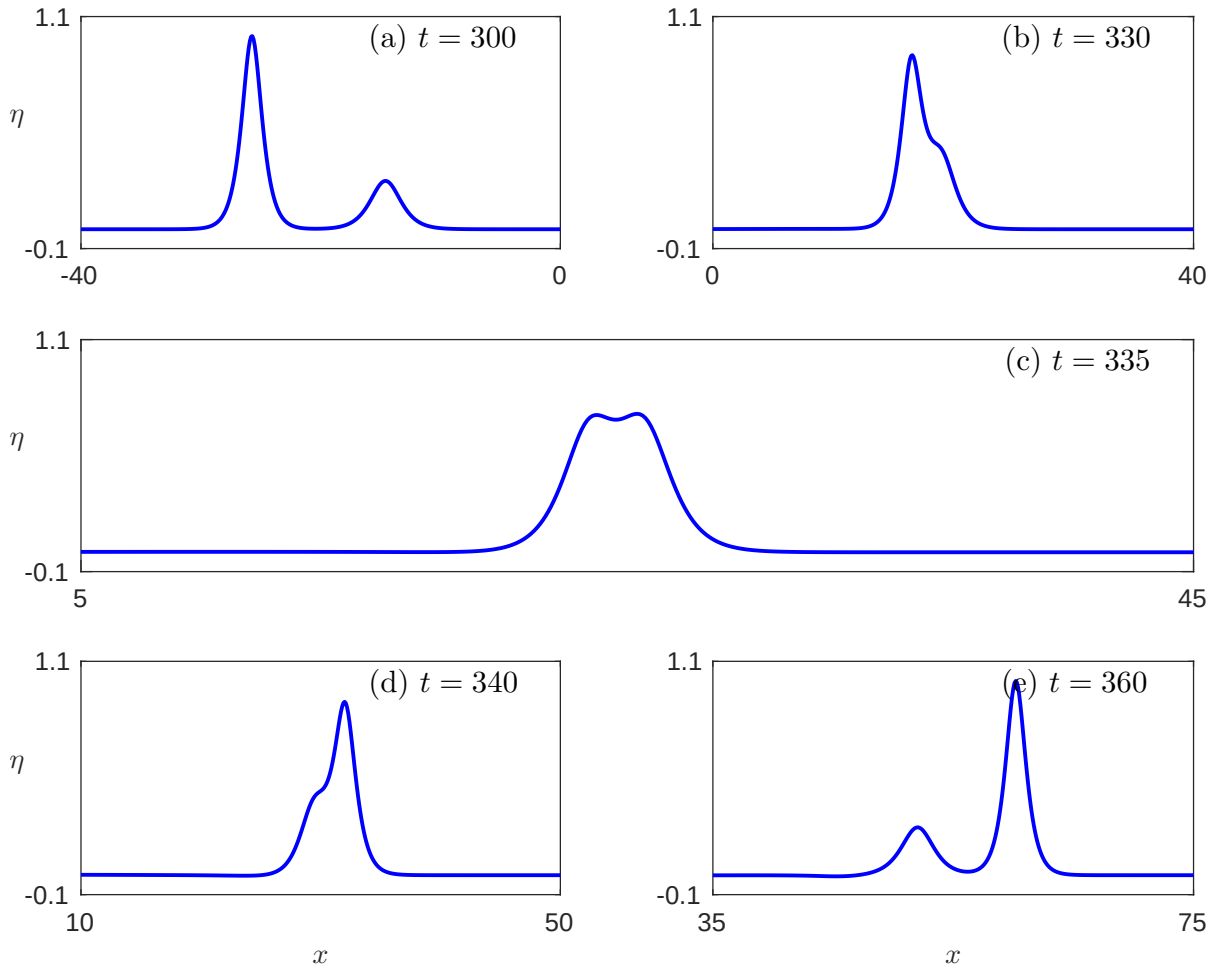

Figure 12. *Interaction of two solitary waves with* $r = 4$ *of the g*Serre *equations with* $B = 0.2$. Lax *category (b).*

values of r. In this Figure, the amplitudes have been translated so as to be all at the same level. Again, we observed that as the interaction changes categories, the maximum amplitude is not a monotone function with respect to r.

The interaction again is inelastic and the generation of small amplitude dispersive tails was observed. Figure 20 shows the dispersive tails generated by the interaction of two solitary waves with $a_1 = -0.1$ and $a_2 = -0.3$. Again, a small amplitude oscillatory dispersive tail was generated in front of the two pulses that travels faster than the pulses. On the other hand, a very fast $N-$shaped wavelet was also generated moving to the left. The tails generated in the other cases where $B > 1/3$ were always very similar thus we do not present them here.

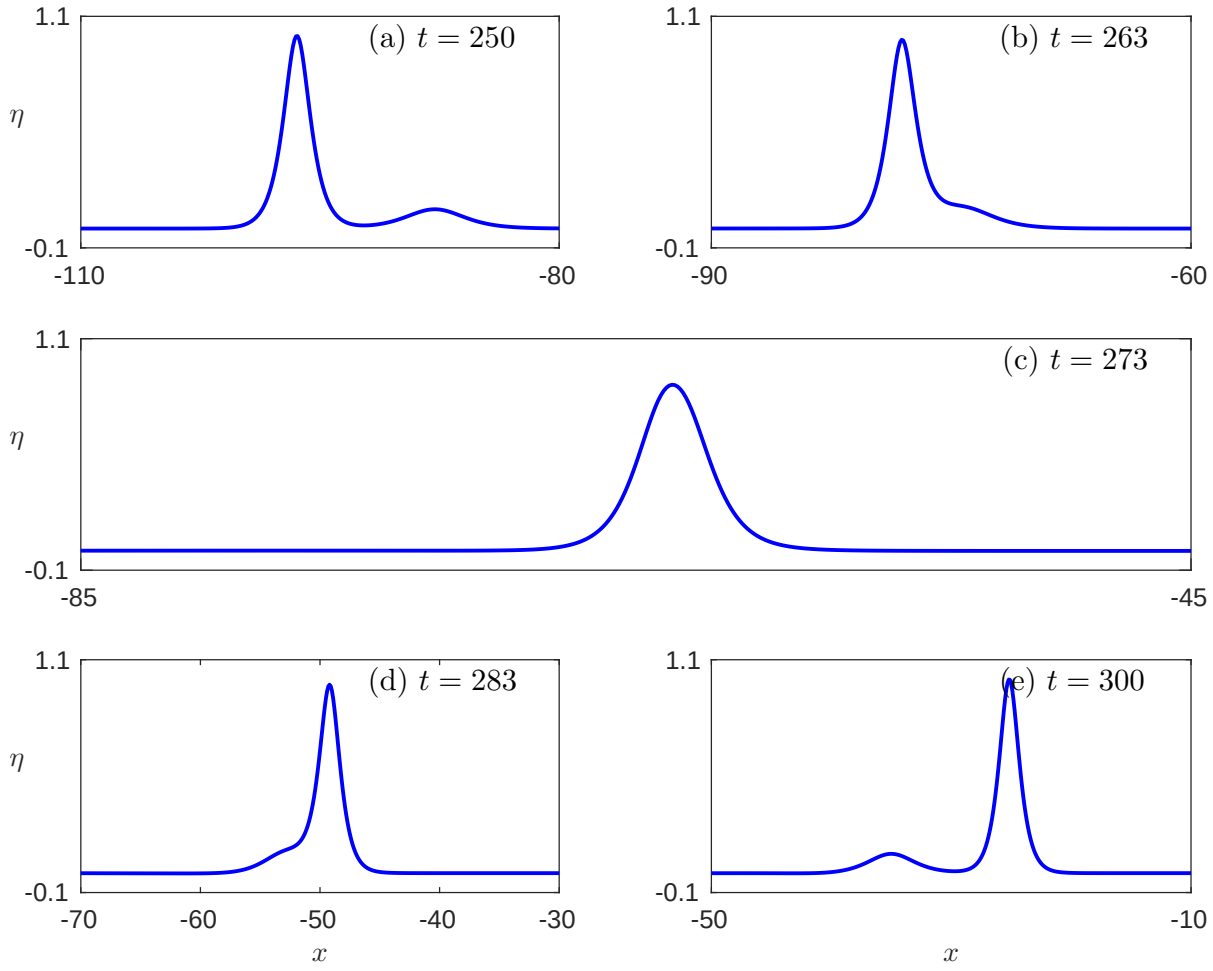

Figure 13. *Interaction of two solitary waves with* $r = 10$ *of the* g Serre *equations with* $B = 0.2$. Lax *category (c).*

3.3. Critical and transcritical cases

In this section, we study the critical case of Bond number $B = 1/3$ and the cases where B is close to this critical value. As it was mentioned in Section 2, and in [17], there are no smooth traveling wave solutions known for the critical Bond number $B = 1/3$ but only the peaked solitary waves given by the formula (2.4). Additionally, the solitary waves corresponding to Bond numbers close to the critical value are very close to peaked solitary waves. Moreover, the behaviour of the solutions for values of $B = 1/3$ is expected to be affected by the absence of dispersive effects. We first study the various interactions of solitary waves in the cases where $B = 0.32$, 0.33, 0.34 and 0.35.

We start with the description of the head-on collision of two equal solitary waves. For the subcritical values of the Bond number, we considered solitary waves of amplitude $A = 1$, while we took $A = -0.3$ for the supercritical values. Although the two waves interact in

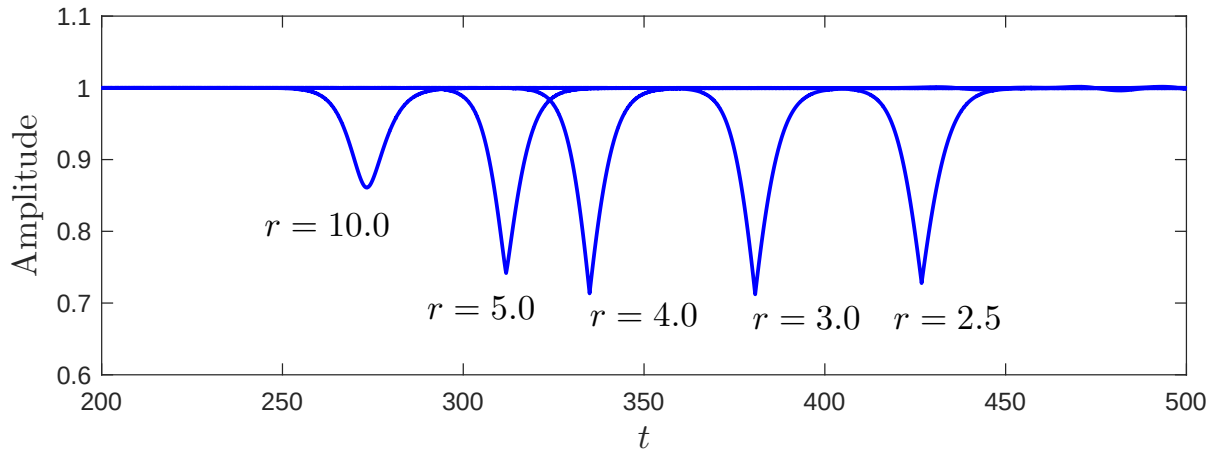

Figure 14. *The amplitude of the solution for several values of r for the overtaking collision of two solitary waves of the g*Serre *equations with* $B = 0.2$.

a similar manner with the cases described in Section 3, the generated dispersive tails are not oscillatory but they are similar to $N-$shaped waves. For example, when $B = 0.34$, the dispersive tail is ahead of the solitary wave, while in the case $B = 0.33$ the tails are behind the solitary waves. A close look at the dispersive tails shows an intermediate state between dispersive and non-dispersive waves. Figure 21 presents the results after the interaction of two equal solitary waves for $B = 0.32$ and $B = 0.34$.

The interactions of solitary waves in all transcritical cases we tested were very similar to the analogous subcritical and supercritical cases. The main difference observed between the two cases was the shape of the dispersive tails. Analogous behavior was observed for the overtaking collision in the transcritical cases. The overtaking collisions generated small $N-$shaped wavelets and dispersive tails, which again consisted of a few oscillations and were very similar to the tails generated after the head-on collision. For this reason, we do not present pictures of the overtaking collisions in the transcritical cases in this paper. We proceed with the critical case $B = 1/3$.

Although the critical case is numerically difficult in the sense that numerical errors might lead to false conclusions, we explored the existence of stable solitary waves when $B = 1/3$. It is known that general initial conditions evolve into a series of solitary waves and dispersive tails in generic nonlinear and dispersive wave models, [3, 17]. In order to examine if the gSerre equations possess stable solitary wave solutions when $B = 1/3$, we tested the evolution of a general initial condition of the form $\eta(x, 0) = a\, e^{-b x^2}$ with zero initial velocity $u(x, 0) = 0$. We present the results for $a = 1$ and $b = 0.1$, *i.e.* when we consider the evolution of a heap of water under gravity. The initial waveform was split into two symmetric waves that eventually evolved into series of solitary waves. In Figures 22(a) and (b) we present the resolution of a Gaussian initial condition into series of solitary waves where we took $\Delta x = 0.02$ and $\Delta t = 0.002$. Although the

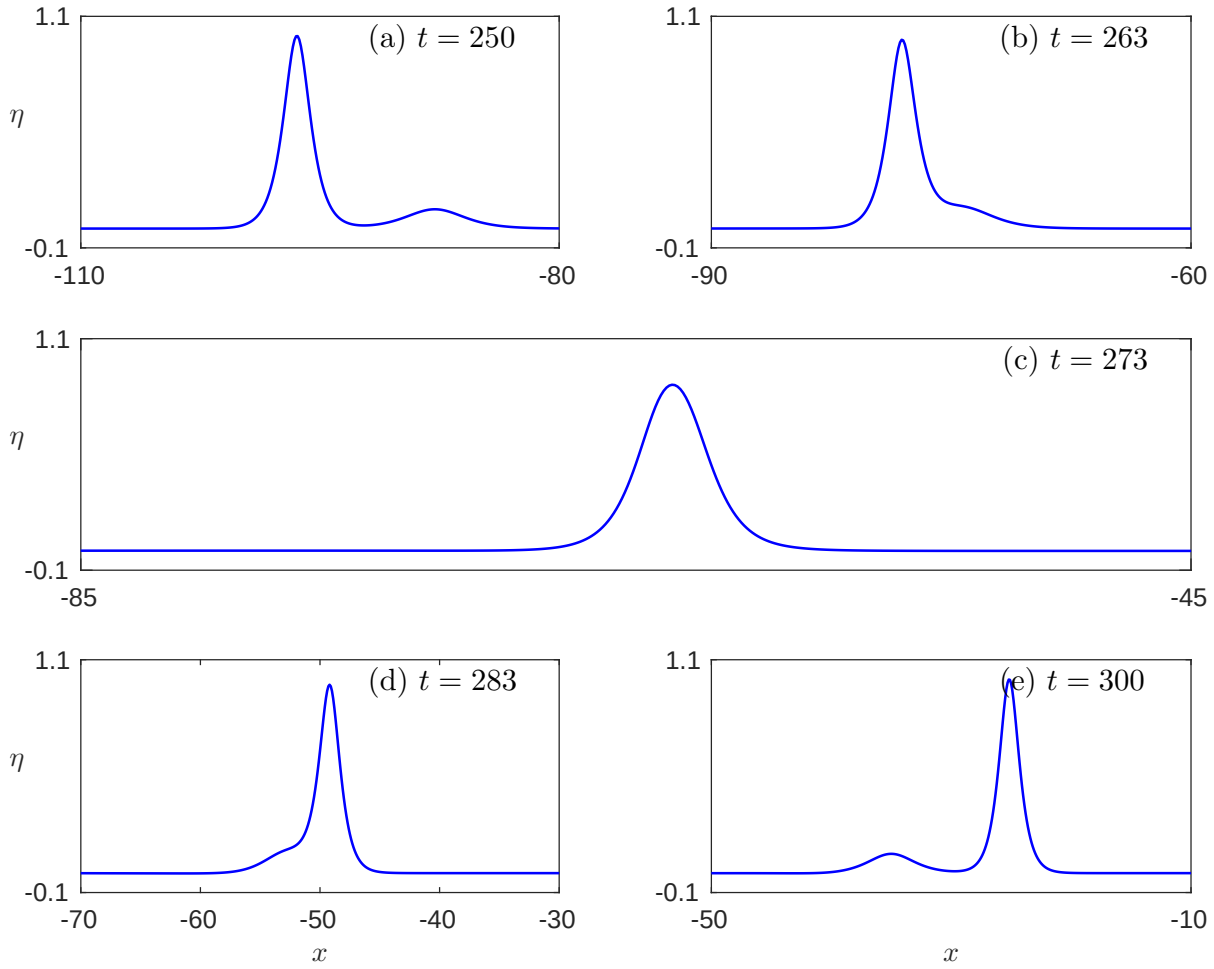

Figure 15. *Dispersive tails generated during the overtaking collision of two solitary waves of the* g*Serre equations with* $B = 0.2$, $r = 4$.

computation was performed in the interval $[-200, 200]$ we present only the solution in the interval $[0, 200]$ because it is symmetric. In Figure 22(b), we observe that the solitary waves coincide with peaked solitary waves when we compare the shape of the numerical solution with the analogous analytical peakon (2.4). This example serves as an indication of the existence of stable peaked solitary waves for the gSerre equations in the critical case $B = 1/3$.

The situation is similar when we take a negative initial condition given by the same formula with $a = -0.5$, $b = 0.1$ for the critical value $B = 1/3$. It was observed that although the initial condition is negative, it resolved into a series of depression peaked solitary waves (also known as antipeakons) indicatiing that the gSerre equations possess both stable depression and elevation peaked solitary waves when $B = 1/3$. In this experiment, we used $\Delta x = 10^{-3}$ and $\Delta t = 10^{-4}$ and again the interval of integration was $[-200, 200]$. Although further theoretical studies are required to ensure the accuracy

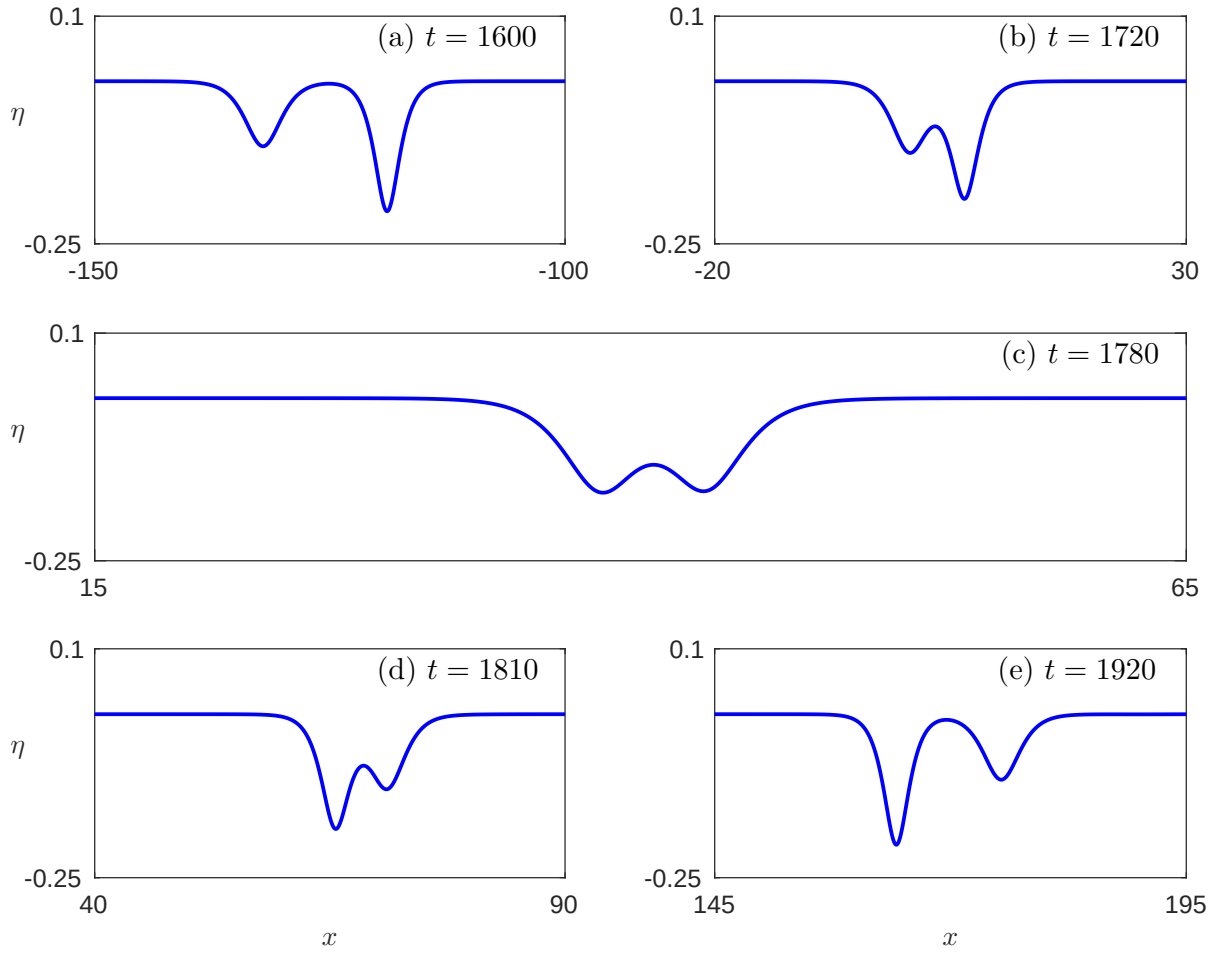

Figure 16. *Interaction of two solitary waves with* $r = 2$ *of the* g*Serre equations with* $B = 0.5$. *Lax category (a).*

of our conclusions, some confidence to the numerical results can be gained by the fact that both elevation and depression traveling waves appear to exist at the same time when $B = 1/3$, contrary to what we have experienced for large and small values of Bond number $B \neq 1/3$ where we were able to compute either elevation or depression solitary waves in each case.

In order to study the solitary waves generated by the evolution of the Gaussian and ensure that they are traveling waves and also that they are peakons in this critical case, we isolated the solitary waves using the cleaning procedure suggested in [3, 18]. After one cleaning iteration, the solitary wave propagated without change in shape, amplitude or speed. Specifically, the elevation solitary wave of Figure 22(a) propagated with constant speed $c_s \approx 1.32$ and amplitude $A \approx 0.7337$. The amplitude of the emerging depression wave was approximately $A \approx -0.3368$. The interaction of the cleaned solutions were studied and found to be very similar to the transcritical cases. The symmetric head-on collision of two elevation peakons is presented in Figure 23 where we observe great

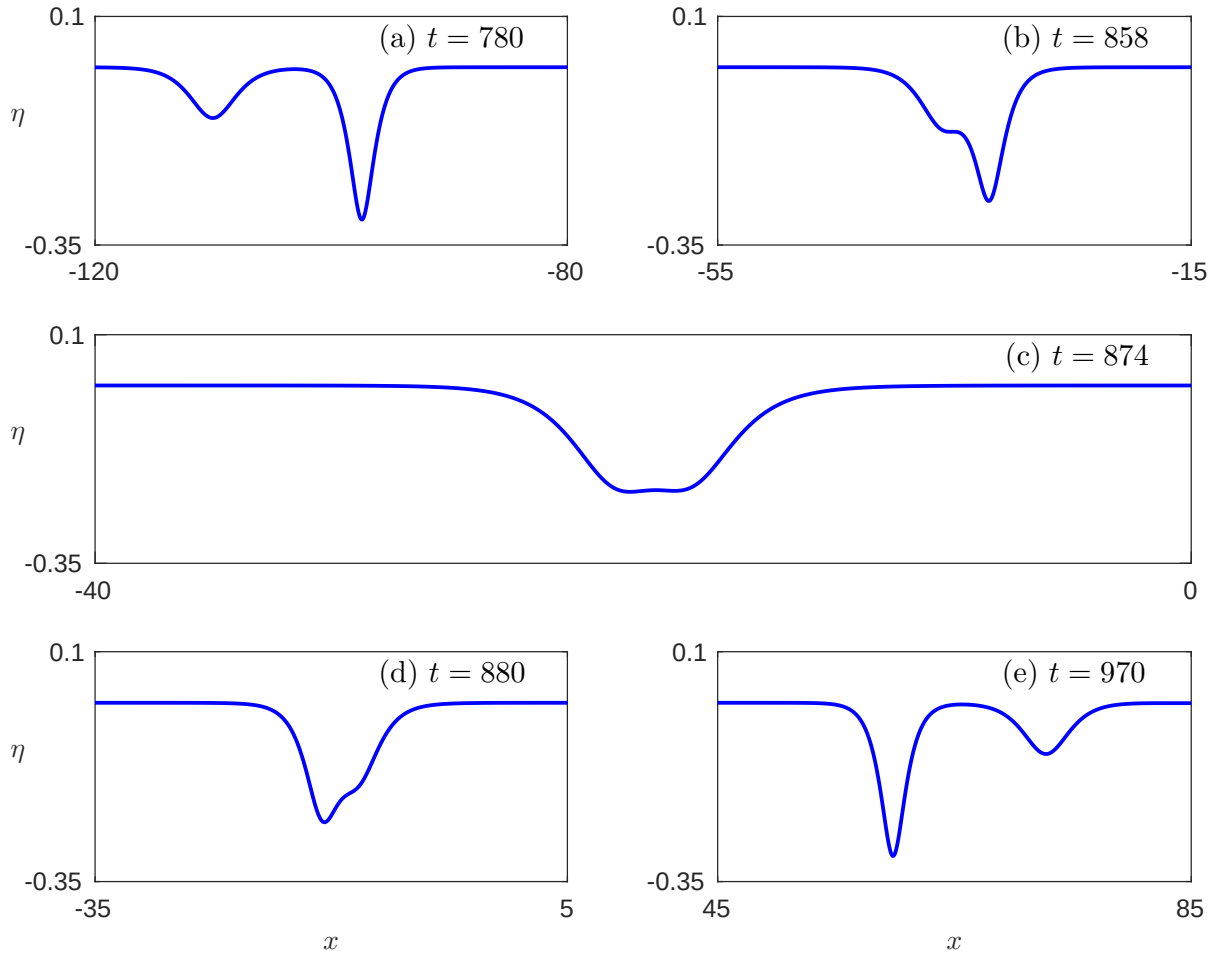

Figure 17. *Interaction of two solitary waves with* $r = 3$ *of the g*Serre *equations with* $B = 0.5$. Lax *category (b).*

similarities with the head-on collision of two solitary waves in the case with $B = 0.32$. Similarly, the head-on collision of two depression peakons leads to very similar results.

We also explored the head-on collision between a peakon of elevation and a peakon of depression with amplitudes $A = 0.5$ and $A = -0.3$, respectively. This collision appeared to be a combination of the two previous collisions. After the interaction, the depression peakon sheds a small wavelet in front of the pulse, leading its propagation while the elevation peakon sheds an analogous wavelet behind, following the propagation of the main pulse. Figure 24 shows the head-on collision between elevation and depression peakons.

The last and also interesting overtaking collision between an elevation and depression peakon is presented in Figure 25. In this experiment, we used the same peakons as in the previous experiment but in this case both of them propagate to the right. The interaction was strong especially for the depression peakon which evolved into a much smaller peakon

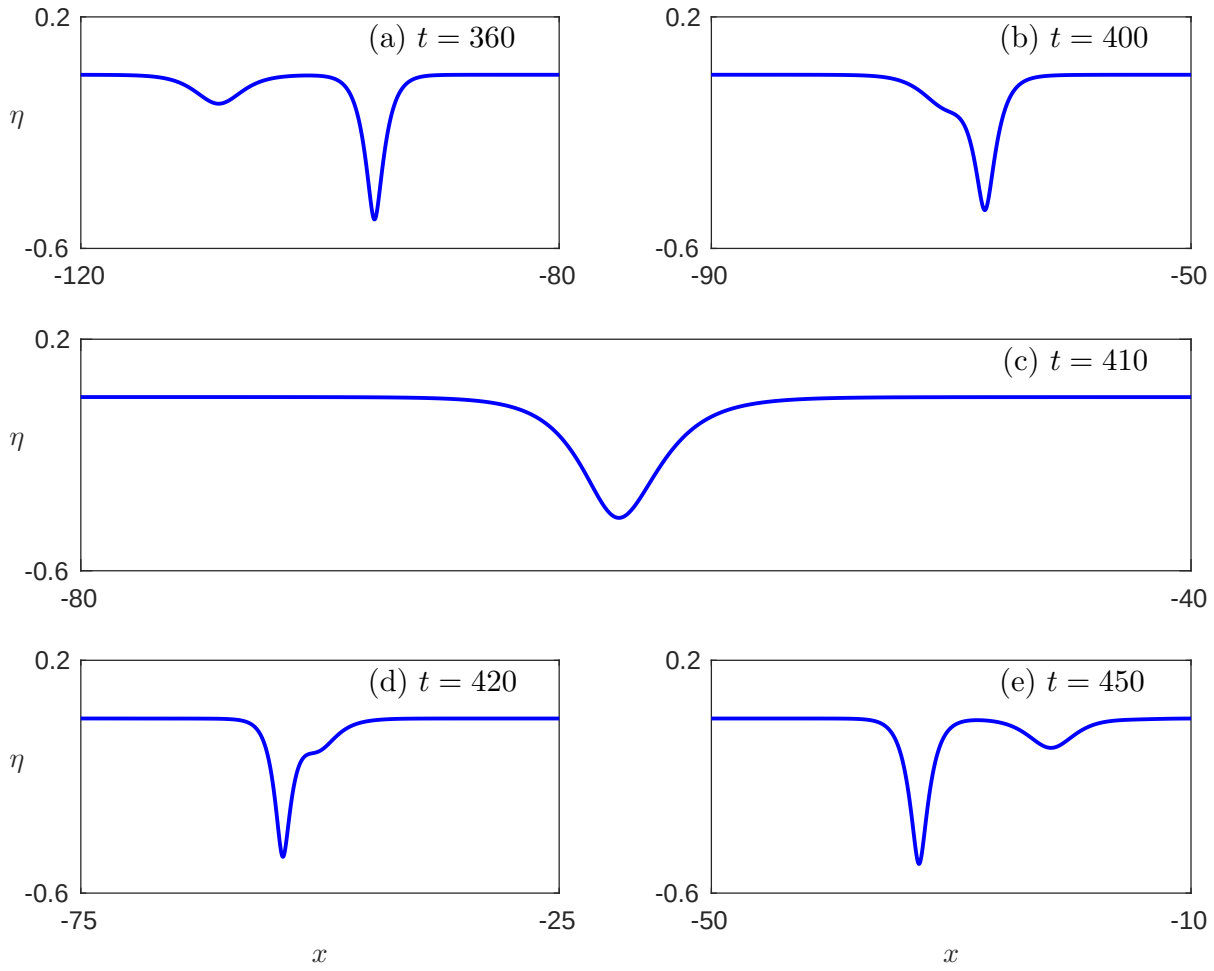

Figure 18. *Interaction of two solitary waves with* $r = 10$ *of the g*Serre *equations with* $B = 0.5$. Lax *category (c).*

while two more peakons were generated after the interaction. Also, other oscillatory structures appeared. The initial elevation peakon evolved into a new elevation peakon of smaller amplitude.

4. Conclusions

Some effects of surface tension on gravity–capillary solitary waves of the gSerre equations were presented. Head-on and overtaking collisions were studied for subcritical and supercritical values of the Bond number. The qualitative dynamical picture of the interactions for values of the Bond number $B < 1/3$ appeared to be very similar to the analogous interactions of solitary waves of the Serre equations that neglect surface tension. The maximum runup was smaller when surface tension was taken into account, and the effect of surface tension was stronger for larger amplitude solitary waves. On the other hand, the

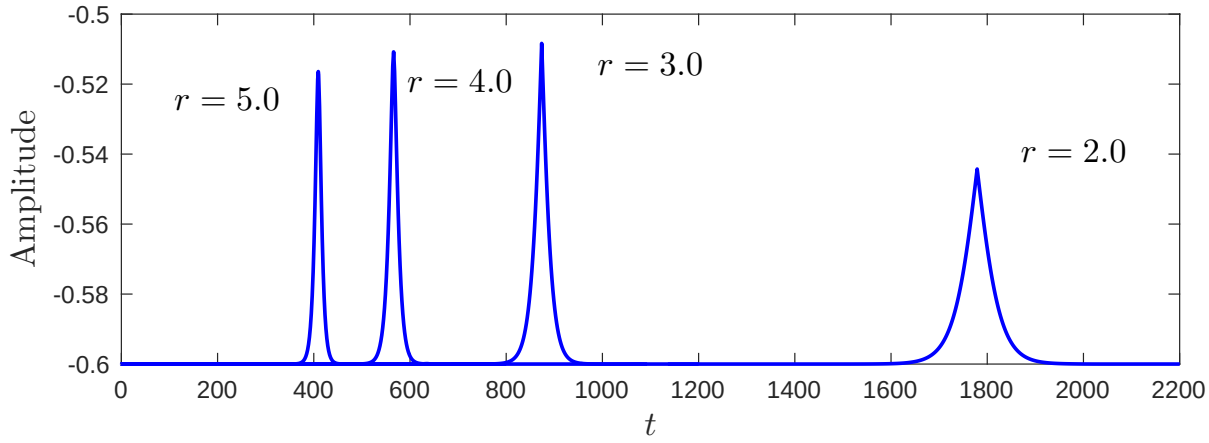

Figure 19. *The maximum negative amplitude of the solution for several values of r for the overtaking collision of two solitary waves of the g*Serre *equations with $B = 0.5$.*

interaction for large values of Bond number $B > 1/3$ were different since the dispersive tails propagate faster than the solitary waves. Finally, we numerically studied the existence of solitary waves in the critical case $B = 1/3$ where the numerical experiments indicated the existence of solitary waves of elevation and depression that are reminiscent of peaked solitary waves of the Camassa–Holm equation. Analytical formulas for these peakons were presented. Finally, we presented the dynamics of solitary waves and their interactions for transcritical and values of the Bond number near $B \approx 1/3$.

Acknowledgments

M. A. Hoefer was partially supported by NSF CAREER DMS-1255422. D. Mitsotakis was supported by the Marsden Fund administered by the Royal Society of New Zealand.

References

[1] D. Antonopoulos, V. Dougalis, and D. Mitsotakis. Error estimates for Galerkin approximations of the Serre equations. *SIAM J. Numer. Anal.*, To appear, 2017. 7, 9, 18, 19

[2] E. Barthélémy. Nonlinear shallow water theories for coastal waves. *Surveys in Geophysics*, 25:315–337, 2004. 6

[3] J. L. Bona and M. Chen. A Boussinesq system for two-way propagation of nonlinear dispersive waves. *Physica D*, 116:191–224, 1998. 24, 26

[4] J. L. Bona, M. Chen, and J.-C. Saut. Boussinesq equations and other systems for small-amplitude long waves in nonlinear dispersive media. I: Derivation and linear theory. *J. Nonlinear Sci.*, 12:283–318, 2002. 4

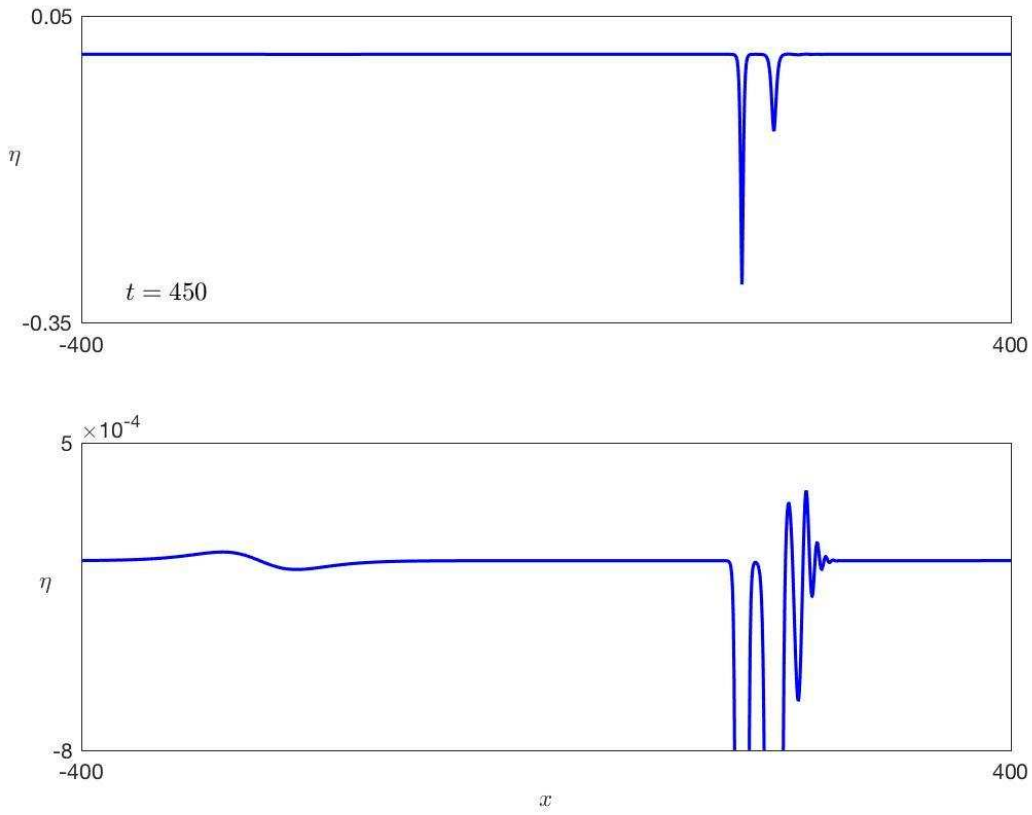

Figure 20. *Dispersive tails generated during the overtaking collision of two solitary waves of the g*Serre *equations with* $B = 0.5$, $r = 3$.

[5] B. Buffoni, M. D. Groves, and J. F. Toland. A Plethora of Solitary Gravity-Capillary Water Waves with Nearly Critical Bond and Froude Numbers. *Phil. Trans. R. Soc. Lond. A*, 354(1707):575–607, mar 1996. 6

[6] R. Camassa and D. Holm. An integrable shallow water equation with peaked solitons. *Phys. Rev. Lett.*, 71(11):1661–1664, 1993. 8, 12

[7] J. Chambarel, C. Kharif, and J. Touboul. Head-on collision of two solitary waves and residual falling jet formation. *Nonlin. Processes Geophys.*, 16:111–122, 2009. 15

[8] Y. Y. Chen, C. Kharif, J. H. Yang, H. C. Hsu, J. Touboul, and J. Chambarel. An experimental study of steep solitary wave reflection at a vertical wall. *Eur. J. Mech. B/Fluids*, 49(A):20–28, jan 2015. 15

[9] D. Clamond, D. Dutykh, and A. Durán. A plethora of generalised solitary gravity-capillary water waves. *J. Fluid Mech.*, 784:664–680, 2015. 4, 5

[10] D. Clamond, D. Dutykh, and A. Galligo. Algebraic method for constructing singular steady solitary waves: a case study. *Proc. R. Soc. Lond. A*, 472(2191), 2016. 4

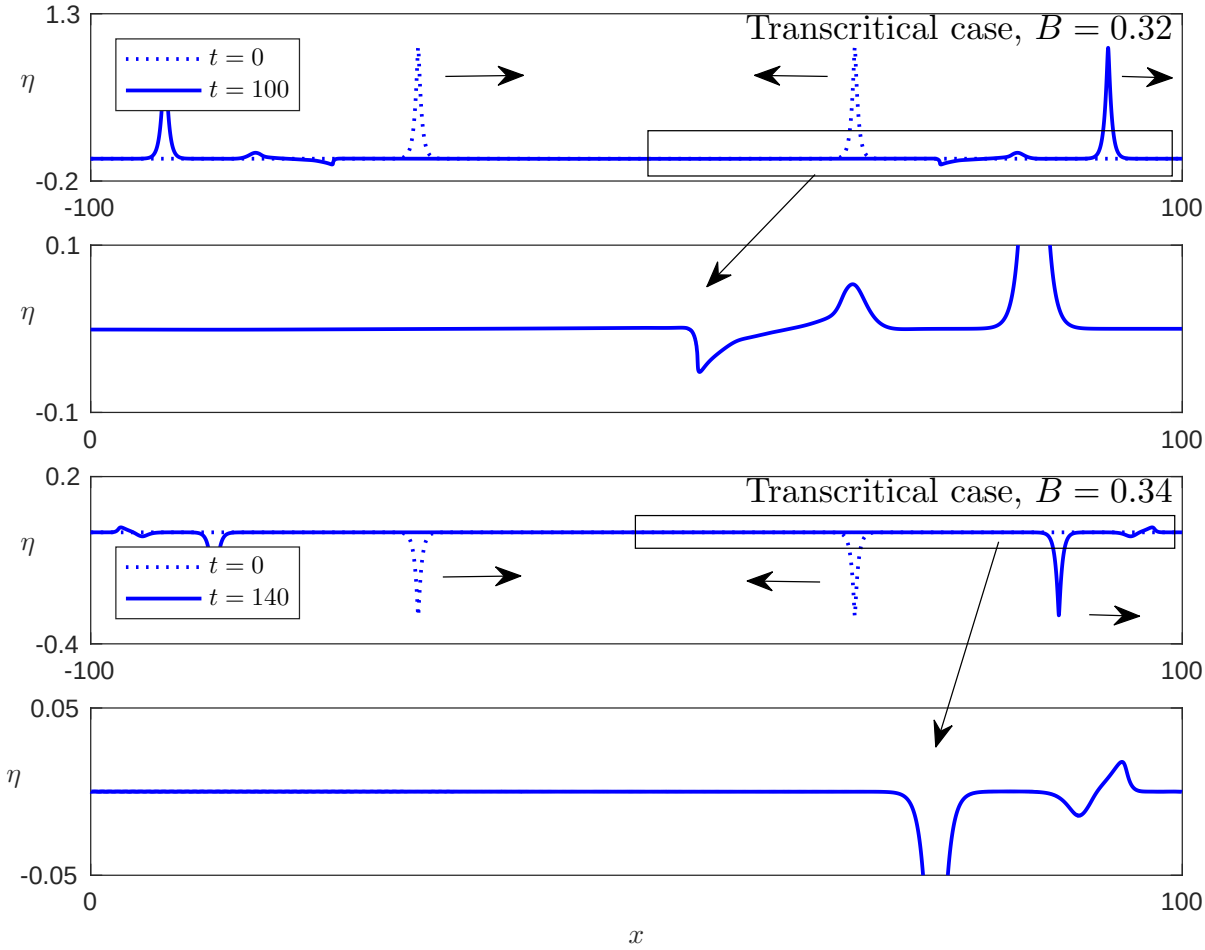

Figure 21. *Head-on collisions of solitary waves of equal amplitude for the transcritical values of* Bond *number* $B = 0.32$ *and* $B = 0.34$.

[11] D. Clamond, D. Dutykh, and D. Mitsotakis. Conservative modified Serre–Green–Naghdi equations with improved dispersion characteristics. *Comm. Nonlin. Sci. Num. Sim.*, 45:245–257, 2017. 4

[12] W. Craig, P. Guyenne, J. Hammack, D. Henderson, and C. Sulem. Solitary water wave interactions. *Phys. Fluids*, 18(5):57106, 2006. 18, 19

[13] P. Daripa and R. K. Dash. A class of model equations for bi-directional propagation of capillary-gravity waves. *Int. J. Eng. Sci.*, 41(2):201–218, jan 2003. 4

[14] R. K. Dash and P. Daripa. Analytical and numerical studies of a singularly perturbed Boussinesq equation. *Appl. Math. Comput.*, 126(1):1–30, feb 2002. 4

[15] F. Dias and C. Kharif. Nonlinear gravity and capillary-gravity waves. *Ann. Rev. Fluid Mech.*, 31:301–346, 1999. 6

[16] F. Dias, D. Menasce, and J.-M. Vanden-Broeck. Numerical study of capillary-gravity solitary waves. *Eur. J. Mech. B/Fluids*, 15(1):17–36, 1996. 6

[17] F. Dias and P. Milewski. On the fully-nonlinear shallow-water generalized Serre equations. *Phys. Lett. A*, 374(8):1049–1053, 2010. 4, 5, 6, 7, 9, 23, 24

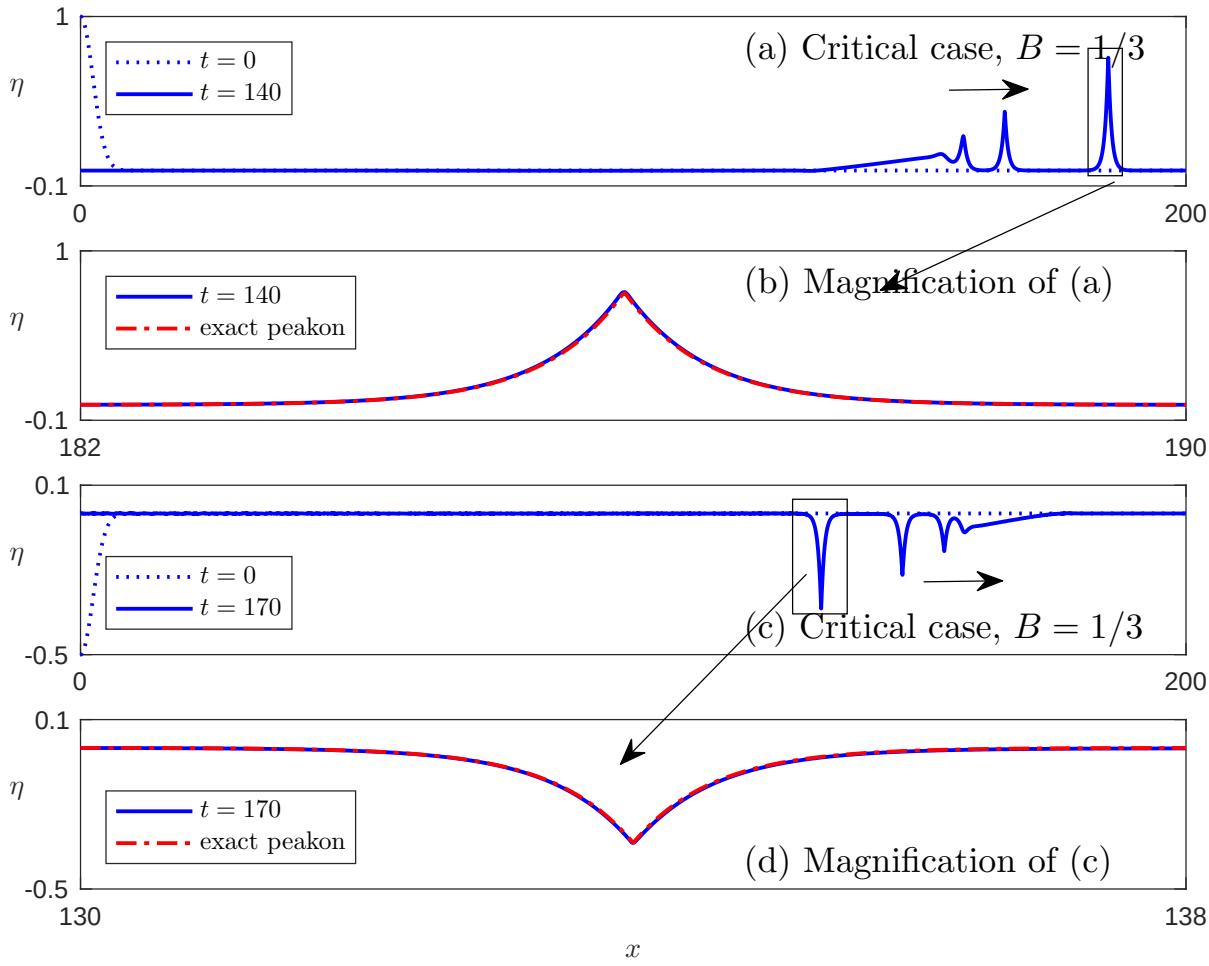

Figure 22. *Evolution of* Gaussian *initial conditions into a series of elevation and depression solitary waves for the critical* Bond *number* $B = 1/3$.

[18] V. A. Dougalis, A. Durán, M. A. Lopez-Marcos, and D. E. Mitsotakis. A numerical study of the stability of solitary waves of Bona-Smith family of Boussinesq systems. *J. Nonlinear Sci.*, 17:595–607, 2007. 26

[19] D. Dutykh, D. Clamond, and A. Durán. Efficient computation of capillary-gravity generalised solitary waves. *Wave Motion*, 65:1–16, sep 2016. 6

[20] G. A. El, R. H. J. Grimshaw, and N. F. Smyth. Asymptotic description of solitary wave trains in fully nonlinear shallow-water theory. *Phys. D*, 237(19):2423–2435, 2008. 6

[21] W. H. Hager. Wilfrid Noel Bond and the Bond number. *J. Hydr. Res.*, 50(1):3–9, feb 2012. 5

[22] J. K. Hunter and J. Scheurle. Existence of perturbed solitary wave solutions to a model equation for water waves. *Phys. D*, 32(2):253–268, sep 1988. 4, 5, 8

[23] T. Kawahara. Oscillatory Solitary Waves in Dispersive Media. *J. Phys. Soc. Japan*, 33(1):260–264, jul 1972. 4

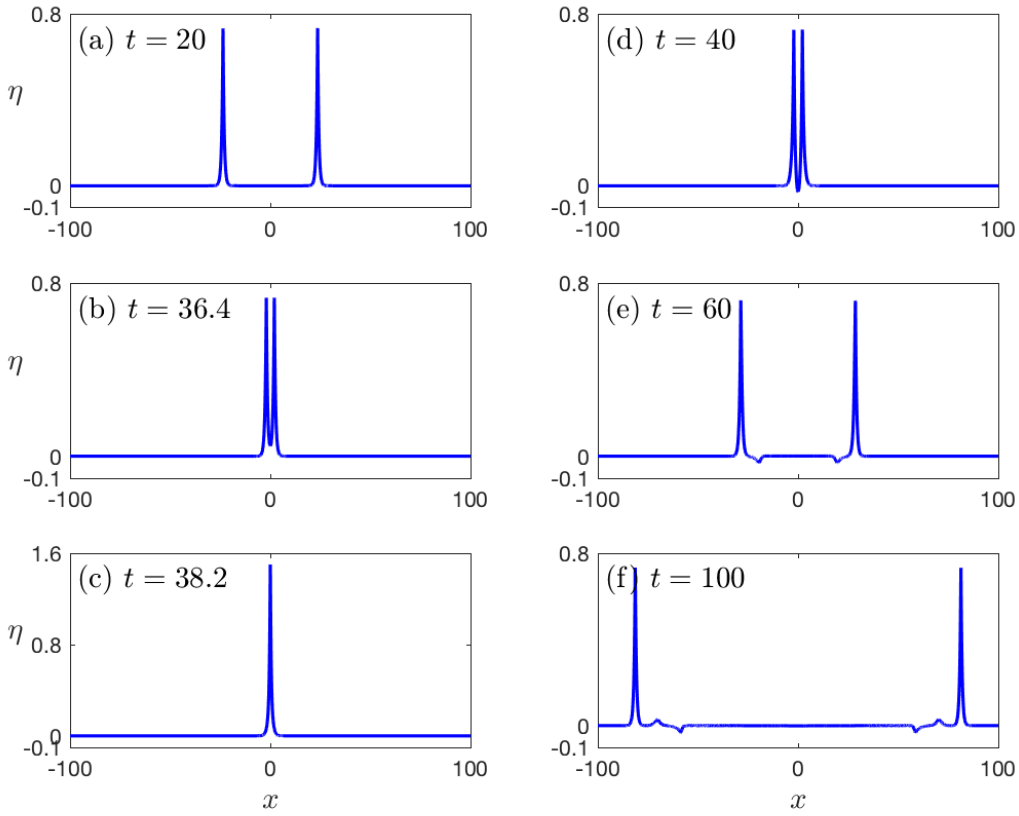

Figure 23. *Head-on collision of cleaned peakons for the critical* Bond *number* $B = 1/3$.

[24] D. Lannes. *The water waves problem: Mathematical analysis and asymptotics*. American Mathematical Society, AMS, 2013. 4

[25] P. D. Lax. Integrals of nonlinear equations of evolution and solitary waves. *Commun. Pure Appl. Math.*, 21:467–490, 1968. 18

[26] Y. A. Li, J. M. Hyman, and W. Choi. A Numerical Study of the Exact Evolution Equations for Surface Waves in Water of Finite Depth. *Stud. Appl. Maths.*, 113:303–324, 2004. 19

[27] S. Liao. Do peaked solitary water waves indeed exist? *Comm. Nonlin. Sci. Num. Sim.*, 19(6):1792–1821, 2014. 12

[28] N. K. Lowman, M. A. Hoefer, and G. A. El. Interactions of large amplitude solitary waves in viscous fluid conduits. *J. Fluid Mech*, 750:372–384, jul 2014. 18

[29] Y. Matsuno. Hamiltonian formulation of the extended Green-Naghdi equations. *Phys. D*, 301-302:1–7, may 2015. 4

[30] J. W. Miles. Obliquely interacting solitary waves. *J. Fluid Mech*, 79(1):157–169, jan 1977. 18

[31] S. M. Mirie and C. H. Su. Collision between two solitary waves. Part 2. A numerical study. *J. Fluid Mech.*, 115:475–492, 1982. 6, 13, 19

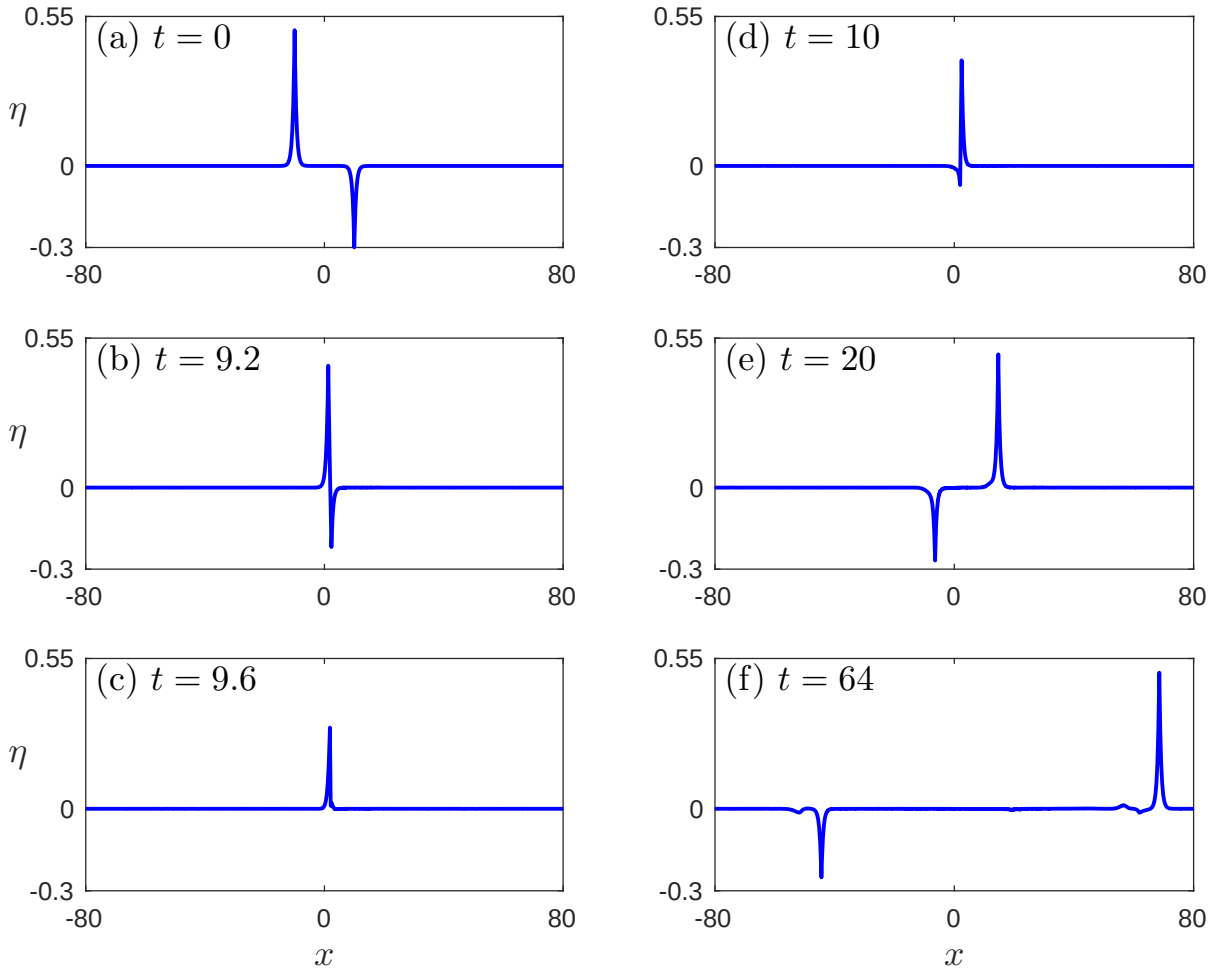

Figure 24. *Head-on collision between elevation and depression peakons for the critical* Bond *number* $B = 1/3$.

[32] D. Mitsotakis, D. Dutykh, A. Assylbekuly, and D. Zhakebaev. On weakly singular and fully nonlinear travelling shallow capillary-gravity waves in the critical regime. *Submitted*, pages 1–16, 2016. 8

[33] D. Mitsotakis, B. Ilan, and D. Dutykh. On the Galerkin/Finite-Element Method for the Serre Equations. *J. Sci. Comput.*, 61(1):166–195, feb 2014. 7, 8, 9, 19

[34] F. Serre. Contribution à l'étude des écoulements permanents et variables dans les canaux. *La Houille blanche*, 8:374–388, 1953. 4, 6

[35] F. Serre. Contribution à l'étude des écoulements permanents et variables dans les canaux. *La Houille blanche*, 8:830–872, 1953. 4, 6

[36] P. Sprenger and M. A. Hoefer. Shock waves in dispersive hydrodynamics with non-convex dispersion. *arXiv:1606.09229*, pages 1–20, 2016. 4, 5, 6

[37] C. H. Su and C. S. Gardner. KdV equation and generalizations. Part III. Derivation of the Korteweg-de Vries equation and Burgers equation. *J. Math. Phys.*, 10:536–539, 1969. 6

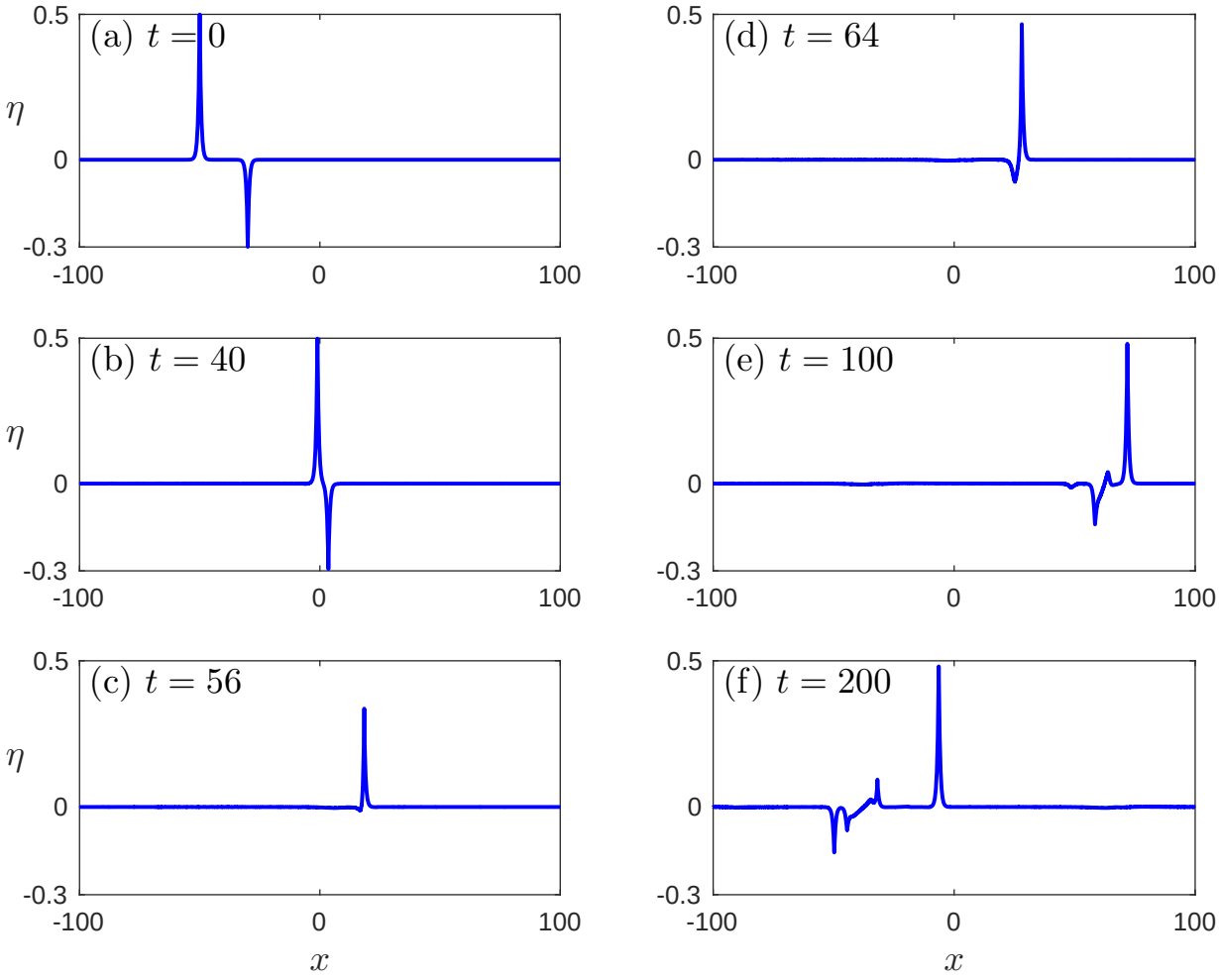

Figure 25. *Overtaking collision between elevation and depression peakons for the critical* Bond *number* $B = 1/3$.

[38] C. H. Su and R. M. Mirie. On head-on collisions between two solitary waves. *J. Fluid Mech.*, 98:509–525, 1980. 13

[39] G. B. Whitham. *Linear and nonlinear waves*. John Wiley & Sons Inc., New York, 1999. 4

D. Dutykh: LAMA, UMR 5127 CNRS, Université Savoie Mont Blanc, Campus Scientifique, F-73376 Le Bourget-du-Lac Cedex, France
E-mail address: Denys.Dutykh@univ-savoie.fr
URL: http://www.denys-dutykh.com/

M. Hoefer: Department of Applied Mathematics, University of Colorado, Boulder, CO, 80309, USA
E-mail address: hoefer@colorado.edu
URL: http://www.colorado.edu/amath/mark-hoefer/

D. Mitsotakis: Victoria University of Wellington, School of Mathematics, Statistics and Operations Research, PO Box 600, Wellington 6140, New Zealand
E-mail address: dmitsot@gmail.com
URL: http://dmitsot.googlepages.com/